

1

2 **A Remediation Approach to Chromium-Contaminated Water and Soil using**  
3 **Engineered Biochar Derived from Peanut Shell**

4

5 **Published in:** *Environmental Research*

6

7 **Citation for published version:** Murad, H.A., Ahmad, M., Bundschuh, J., Hashimoto, Y., Zhang,  
8 M., Sarkar, B., Ok, Y.S., (2022) A Remediation Approach to Chromium-Contaminated Water and  
9 Soil using Engineered Biochar Derived from Peanut Shell. *Environmental Research*, 204: 112125.  
10 doi: 10.1016/j.envres.2021.112125.

11

12 **Document version:** Accepted peer-reviewed version.

13 **A Remediation Approach to Chromium-Contaminated Water and Soil using Engineered**  
14 **Biochar Derived from Peanut Shell**

15

16 Hafiza Afia Murad<sup>a,1</sup>, Mahtab Ahmad<sup>a,1,\*</sup>, Jochen Bundschuh<sup>b</sup>, Yohey Hashimoto<sup>c</sup>, Ming Zhang<sup>d</sup>, Binoy  
17 Sarkar<sup>e</sup>, Yong Sik Ok<sup>f,\*</sup>

18

19 <sup>a</sup> Department of Environmental Sciences, Faculty of Biological Sciences, Quaid-i-Azam University,  
20 Islamabad 45320, Pakistan

21 <sup>b</sup> UNESCO Chair on Groundwater Arsenic within the 2030 Agenda for Sustainable Development,  
22 University of Southern Queensland, West Street, Toowoomba, Queensland 4350, Australia

23 <sup>c</sup> Department of Bio-Applications and Systems Engineering, Tokyo University of Agriculture and  
24 Technology, 2-24-16 Koganei, Tokyo 184-8588, Japan

25 <sup>d</sup> Department of Environmental Engineering, China Jiliang University, No. 258 Xueyuan Street, Hangzhou,  
26 Zhejiang 310018, China

27 <sup>e</sup> Lancaster Environment Center, Lancaster University, Lancaster, LA1 4YQ, United Kingdom

28 <sup>f</sup> Korea Biochar Research Center, APRU Sustainable Waste Management Program & Division of  
29 Environmental Science and Ecological Engineering, Korea University, Seoul, Korea

30

31

32

33 <sup>1</sup> These authors share co-first authorship.

34

35 \* Corresponding authors

36 Email: [mahmad@qau.edu.pk](mailto:mahmad@qau.edu.pk) (Mahtab Ahmad); [yongsikok@korea.ac.kr](mailto:yongsikok@korea.ac.kr) (Yong Sik Ok)

37

## 38 **Highlights**

- 39 • Peanut shells were converted to biochar, and engineered with CTAB
- 40 • High Cr(VI) removal efficiency for the engineered biochar (79.35%) was observed
- 41 • Chemisorption was the main mechanism of interaction between Cr(VI) and the biochar
- 42 • High immobilization of Cr(VI) was observed in the soil with engineered biochar

43

## 44 **Abstract**

45 Hexavalent chromium (Cr(VI)) is one of the major environmental concerns due to its excessive discharge  
46 through effluents from the leather tanning industry. Peanut production leads to the generation of residual  
47 shells as waste calling for sustainable disposal. In this study, we employed an innovative approach of  
48 applying peanut-shell-derived pristine and engineered biochar for the remediation of Cr-contaminated  
49 wastewater and soil. The peanut shell waste was converted to biochar, which was further engineered with  
50 cetyltrimethylammonium bromide (CTAB, a commonly used cationic surfactant). The biochars were then  
51 used for the adsorption and immobilization of Cr(VI) in water and soil, respectively. The adsorption  
52 experiments demonstrated high Cr(VI) removal efficiency for the engineered biochar (79.35%) compared  
53 with the pristine biochar (37.47%). The Langmuir model best described the Cr(VI) adsorption onto the  
54 biochars ( $R^2 > 0.97$ ), indicating monolayer adsorption. Meanwhile, the adsorption kinetics indicated that  
55 chemisorption was the dominant mechanism of interaction between the Cr(VI) and the biochars, as  
56 indicated by the best fitting to the pseudo-second-order model ( $R^2 > 0.98$ ). Adsorption through the fixed-  
57 bed column also presented higher Cr(VI) adsorption onto the engineered biochar ( $q_{eq} = 22.93 \text{ mg g}^{-1}$ ) than  
58 onto the pristine biochar ( $q_{eq} = 18.54 \text{ mg g}^{-1}$ ). In addition, the desorption rate was higher for the pristine  
59 biochar column ( $13.83 \text{ mg g}^{-1}$ ) than the engineered biochar column ( $10.45 \text{ mg g}^{-1}$ ), indicating that Cr(VI)  
60 was more strongly adsorbed onto the engineered biochar. A higher immobilization of Cr(VI) was observed  
61 in the soil with the engineered biochar than with the pristine biochar, as was confirmed by the significant  
62 decreases in the Cr(VI) bioavailability (92%), leachability (100%), and bioaccessibility (97%) compared

63 with the control (soil without biochar). The CTAB-engineered biochar could thus potentially be used as an  
64 efficient adsorbent for the removal and the immobilization of Cr(VI) in water and soil, respectively.

65  
66 **Keywords:** Designer biochar; Soil quality; Soil remediation; Sustainable Development Goals; Life on land

## 67 68 **1. Introduction**

69 Chromium (Cr), which generally exists in trivalent or hexavalent form, is discharged through the leather  
70 tanning, metal processing, mining, and electroplating industries, causing severe contamination to water,  
71 soil, and plants worldwide (Rajapaksha et al., 2018). Specifically, the wastewater from leather tanning  
72 industry can contain 1,500–3,000 mg L<sup>-1</sup> Cr (Sabur et al., 2013), and there has been a global increase in Cr  
73 concentrations in water bodies pertaining to this industry. High concentrations of up to 84, 50, and 60 µg  
74 L<sup>-1</sup> Cr in surface water, groundwater, and drinking water, respectively, have been reported in major  
75 countries around the globe, while the permissible limit is 0.5–2 µg L<sup>-1</sup> (Jobby et al., 2018). The hexavalent  
76 chromium (Cr[VI]) is around 500 times more toxic than trivalent chromium (Cr[III]), and can cause  
77 carcinogenesis, teratogenesis, and mutations in living bodies (Chen et al., 2015). In fact, Cr(VI) is included  
78 in the United States Environmental Protection Agency’s list of top-priority hazardous pollutants (US-EPA,  
79 2014).

80 Soil is a major sink for heavy metals released into the environment via anthropogenic activities such as the  
81 disposal of tannery waste and various activities pertaining to the metallurgy industry. Globally, 896 tons of  
82 Cr is disposed of each year into soils (Mohan and Pittman, 2006). Irrigation through metal-contaminated  
83 wastewater and sludge application is also causing the contamination of soil and various crops, and their  
84 long-term persistence is somewhat alarming (Kumar et al., 2005). Specifically, tannery sludge contains  
85 4.2% of Cr (Xia et al., 2019), largely comprised of extremely mobile fractions, which consequently poses  
86 the threat of soil and water contamination in the nearby areas (Riaz et al., 2020). There is thus an urgent  
87 need to design cost-effective and simple technology to remove Cr(VI) from the wastewater in water bodies  
88 as well as from soil (Palansooriya et al., 2020).

89 The available techniques for industrial wastewater treatment are adsorption, ion exchange, chemical  
90 precipitation, oxidation/reduction, and membrane separation (e.g., reverse osmosis and ultrafiltration)  
91 (Wang et al., 2019). Meanwhile, soil washing, immobilization, phytoremediation, soil extraction, and  
92 vitrification are among the available treatment technologies for heavy-metal-contaminated soils (Fytianos  
93 et al., 2000). The carbon-based adsorbents have been reported as efficient means of remediating the metal-  
94 contaminated water and soil (Hilber and Bucheli, 2010; Yang et al., 2019). Biochar, a carbon-rich material  
95 obtained from the thermal processing of bio-waste, has recently emerged as a promising adsorbent for  
96 wastewater treatment and a promising soil amendment (El-Naggar et al., 2018a).

97 Bio-waste will ideally produce biochar in such a way that it reduces the waste burden and helps in the area  
98 of waste management. In fact, this can lead to achieving sustainable development goals (set by the General  
99 Assembly of the United Nations) in terms of good health and well-being (Goal 3), clean water and sanitation  
100 (Goal 6), climate action (Goal 13), and life on land (Goal 15) (Kumar and Bhattacharya, 2020). Peanut  
101 shells are generated as waste following the peanuts' consumption as food. It is estimated that 1.6 ton ha<sup>-1</sup>  
102 of peanut shell waste is produced worldwide (Torkashvand et al., 2015). Specifically, in Pakistan, 18,280  
103 ton yr<sup>-1</sup> of peanut shell waste is generated, with the total peanut production amounting to 91,400 ton yr<sup>-1</sup>  
104 (PARC, 2020). The peanut shells are largely burned in the open atmosphere, causing greenhouse gas  
105 emissions, or become buried in soil, with a slow degradation rate (Duc et al., 2019). Unlike other biowaste  
106 types, peanut shells are not decomposed easily in the environment because of their high lignin contents.  
107 Additionally, peanut shells exhibit adsorption potential for heavy metals such as Cu, Ni, Zn, and Cr (Duc  
108 et al., 2019). To avoid environmental issues related to peanut shells waste disposal and to synthesize an  
109 efficient adsorbent, the material could be a valuable feedstock for biochar production. Various recent  
110 studies have reported biochar's efficacy in terms of Cr(VI) removal from water (Rajapaksha et al., 2018;  
111 Huang et al., 2020) and Cr(VI) immobilization in soil (Rafique et al., 2020; Khan et al., 2020). However,  
112 an innovative and systematic approach of applying peanut-shell-derived biochar for the remediation of Cr-  
113 contaminated water and soil has, as yet, not been reported.

114 A common restraint in the application of pristine biochar is its relatively low efficiency for contaminant  
115 mitigation, which has led to the engineering of biochar surfaces to remediate metal-contaminated water and  
116 soil (Zhang et al., 2020; Wang et al., 2020). Biochar can be engineered via acid/base, magnetic, steam,  
117 amine, or surfactant treatments, depending on the desired properties of the engineered product (Rajapaksha  
118 et al., 2016). Specifically, ionic surfactants can easily bind onto the biochar surfaces to facilitate the  
119 electrostatic interaction with the ionic contaminants (Saleh, 2006). However, the biochar surface is  
120 generally negatively charged ( $\text{pH}_{\text{PZC}} < 7$ ; Li et al., 2017), which means pristine biochar may not be effective  
121 in removing anionic forms of metals (e.g., chromate  $[\text{CrO}_4^{2-}]$  and dichromate  $[\text{Cr}_2\text{O}_7^{2-}]$ ) due to electrostatic  
122 repulsion. Engineering the biochar with a cationic surfactant may alter the biochar surface from a negative  
123 to a positive charge (El-Naggar et al., 2018b). The resulting engineered biochar will have the potential  
124 capacity for effectively removing anionic forms of metal such as  $\text{CrO}_4^{2-}$  (Cr[VI]) from water, while it could  
125 also reduce the mobility of Cr(VI) in soil.

126 Cetyltrimethylammonium bromide (CTAB) is a cationic surfactant that can be used for biochar engineering  
127 due to its reported ability to increase the positive charge on the biochar surface (Mathurasa and  
128 Damrongsiri, 2017; Li et al., 2018). Moreover, surfactants tend to be commonly used household chemicals,  
129 and are thus easily available for biochar engineering purposes. It is hypothesized that the Cr(VI) in its  
130 anionic form could be attracted by the positively charged micelles of the CTAB anchored on biochar, which  
131 will enable the on-site covalent bonding with Cr(VI). Hence, the present study was aimed at developing an  
132 innovative approach to remediating the Cr(VI)-contaminated wastewater and soil impacted by tannery  
133 industry using CTAB-engineered biochar derived from peanut shells. Furthermore, we also evaluated the  
134 Cr(VI) remediation potentials by comparing the efficacy of pristine and engineered biochars.

135

## 136 **2. Materials and methods**

### 137 **2.1. Preparation, engineering, and characterization of biochar**

138 Peanut shells were collected from household waste and university campus residential areas. The feedstock  
139 was chopped to a small particle size and subjected to pyrolysis for biochar production. The biochar was

140 produced by pyrolyzing the processed peanut shells in a muffle furnace (Vulcan D-550, USA) under limited  
141 oxygen conditions at a heating rate of  $6^{\circ}\text{C min}^{-1}$ . The carbonization process temperature was fixed at  $600^{\circ}\text{C}$ ,  
142 with the heating continued at this temperature for 2 h. The resulting pristine biochar (PBC) was allowed to  
143 cool at room temperature and was then stored in zipper bags to prevent moisture until used.

144 For the engineering of the biochar, we adopted the chemical modification process reported by Mi et al.  
145 (2016). In brief, the biochar was first acid-washed with 4 M HCl solution for 12 h to remove any minerals  
146 before being separated via filtration using Whatman 42 filter paper. The filtered biochar was then washed  
147 with distilled water several times to achieve a neutral pH before being dried overnight in an oven at  $80^{\circ}\text{C}$ .  
148 Following this, the demineralized biochar was added into 1% CTAB solution at a rate of 1% wt/vol. The  
149 mixture was then stirred at 700 rpm for 24 h using a magnetic stirrer. The suspension was then filtered  
150 through Whatman 42 filter paper to obtain the solid product, which was then oven-dried at  $80^{\circ}\text{C}$  overnight.  
151 The final engineered biochar (EBC) product was then stored in an airtight container for further analysis and  
152 application.

153 The produced biochars (PBC and EBC) were subjected to proximate analysis (moisture, mobile matter,  
154 resident matter, and ash), as well as pH, electrical conductivity (EC), organic matter, scanning electron  
155 microscopy (SEM), and Fourier transform infrared (FTIR) spectroscopy analyses. The proximate and  
156 chemical analytical procedures were carried out with reference to Ahmad et al. (2012a). Various SEM  
157 images of the biochar surfaces were taken using a JSM-6490A, JEOL (Japan) microscope, while the  
158 Spectral 65 Perkin Elmer (USA) FTIR instrument was used for the determination of the functional groups  
159 on the biochar surfaces. The pH point of zero charges ( $\text{pH}_{\text{PZC}}$ ) of the biochars was determined following  
160 the method reported by Xu et al. (2019). Briefly, a 0.1 g biochar sample was stirred in 50 mL of 0.01 M  
161  $\text{CaCl}_2$  solution, the pH of which was adjusted with values ranging from 2 to 12 (with 0.5 M HCl or NaOH  
162 solutions) for 24 h at 120 rpm. The  $\text{pH}_{\text{PZC}}$  was calculated by plotting the  $\Delta\text{pH}$  (difference in final and initial  
163 pH) against the initial pH values.

164

165 **2.2. Wastewater and soil collection, processing, and characterization**

166 Soil and wastewater samples were collected from a tannery industry zone located near Sialkot, Pakistan.  
167 The wastewater samples were collected from the disposal point of the industrial zone in pre-cleaned plastic  
168 bottles and were subsequently filtered through Whatman 42 filter paper to remove any suspended particles.  
169 The soil samples were collected from a radius of 1 km surrounding the industrial zone, with the top 15–20  
170 cm of soil grabbed from different points. A composite sample was then produced by mixing and  
171 homogenizing the grab samples in a polythene sack. The samples were preserved either in pre-cleaned  
172 plastic bottles or bags at 4°C prior to the laboratory analysis. The soil was air-dried and sieved through a 2-  
173 mm aperture to remove any gravel or other rubble and to ensure homogenized soil particles were obtained.  
174 The total amount of Cr in the wastewater samples was measured following the acid digestion method  
175 (method 3005a; US-EPA 1992a) using an atomic absorption spectrometer (AAS; SpectrAA-220, Varian,  
176 USA). The presence of Cr(VI) was determined colorimetrically (method 7196a; US-EPA 1992b) using  
177 diphenyl carbazide with a UV-visible spectrophotometer (Bio-Rad UV3000, USA). The total  
178 concentrations of Cr and Cr(VI) in the wastewater samples were  $40.83 \pm 3.52$  and  $24.86 \pm 0.23$  mg L<sup>-1</sup>,  
179 respectively. Meanwhile, the soil was characterized in terms of general soil parameters (pH, EC, texture,  
180 organic matter, etc.) following the methods reported by Estefan et al. (2013), and total Cr concentration  
181 following the acid digestion method (method 3050; US-EPA 1992c) using the AAS. The soil was acidic  
182 (pH  $5.00 \pm 0.02$ ) with a silt loam texture. The total Cr and Cr(VI) concentrations in the soil were  $1992.23$   
183  $\pm 19.20$  and  $212.88 \pm 15.06$  mg kg<sup>-1</sup> (see Table S1 in the supplementary material).

184

### 185 **2.3. Equilibrium adsorption experiments**

186 The biochars (PBC and EBC) were tested for their adsorption capacities in terms of aqueous Cr(VI)  
187 removal. Here, batch-type equilibrium isotherm and kinetics experiments were performed. First, potassium  
188 dichromate (K<sub>2</sub>Cr<sub>2</sub>O<sub>7</sub>) was used to prepare a stock solution of 500 mg L<sup>-1</sup> Cr(VI) in deionized water. A  
189 series of concentrations, including 5, 10, 25, 50, 150, and 300 mg L<sup>-1</sup>, were then prepared for the  
190 equilibrium adsorption experiments. A relatively high concentration range of Cr(VI) (0–300 mg L<sup>-1</sup>) was  
191 selected due to the high average concentration (~ 400 mg L<sup>-1</sup>) reported in the wastewater of different local

192 tannery industries in Pakistan (Bhalli and Khan, 2006). For each batch experiment, a 45 mL solution of  
193 each concentration was taken in a 50 mL falcon tube, with the biochar dose fixed at a rate of 2 g L<sup>-1</sup>. Then,  
194 the samples were shaken using a horizontal shaker at 110 rpm at room temperature for 24 h. Following this,  
195 the solutions were filtered through Whatman 42 filter paper, and the Cr(VI) concentration in the aqueous  
196 phase was determined. Control samples (without biochar) were also used for each batch experiment. All  
197 experiments were performed in triplicate. The amount of adsorbed contaminant was calculated using the  
198 following equation (Volesky, 2007):

199

$$200 \quad Q_e = (C_o - C_e) \times v/w$$

201

202 where  $Q_e$  is the amount of Cr(VI) (mg g<sup>-1</sup>) adsorbed by the biochar at equilibrium,  $C_o$  is the initial Cr(VI)  
203 concentration in the solution,  $C_e$  is the remaining concentration in the solution at equilibrium,  $v$  is the  
204 volume of the solution (L), and  $w$  is the weight of the biochar (g). The Cr(VI) removal efficiency of each  
205 biochar was calculated using the following equation:

206

$$207 \quad \text{Removal (\%)} = \left( \frac{C_o - C_e}{C_o} \right) \times 100$$

208

209 Three isotherm models, the Freundlich, Langmuir, and Temkin models, were employed to optimize the  
210 usage efficiency of the biochar. The Freundlich model describes the adsorption on the heterogeneous  
211 surface and the multilayer adsorption and is expressed by the following equation (Tran et al., 2017):

212

$$213 \quad Q_e = K_F C_e^N$$

214

215 where  $K_F$  is the capacity of the adsorbent to sorb the adsorbate (mg g<sup>-1</sup>) and  $N$  is the parameter pertaining  
216 to the linearity. Meanwhile, the Langmuir model explicates the adsorption on a homogeneous surface and

217 defines the monolayer adsorption on the surface of the adsorbents according to the following equation (Tran  
218 et al., 2017):

219

$$220 \quad Q_e = Q_{\max} K_L C_e (1 + K_L C_e)^{-1}$$

221

222 where  $Q_{\max}$  is the maximum amount of Cr(VI) adsorbed ( $\text{mg g}^{-1}$ ) and  $K_L$  is the adsorption equilibrium  
223 constant ( $\text{L mg}^{-1}$ ). Finally, the Temkin isotherm model is specifically related to the adsorption heat,  
224 providing evidence regarding the effects of any indirect adsorbate/adsorbate connections on the adsorption  
225 process. In short, the model assesses how the heat of adsorption of all the molecules in the layer decreases  
226 linearly due to the increase in surface coverage, which can be articulated using the following equation  
227 (Ahmad et al., 2013a):

228

$$229 \quad Q_e = \frac{RT}{B} \ln(A C_e)$$

230

231 where  $R$ ,  $T$ ,  $B$ , and  $A$  are the universal gas constant ( $8.314 \text{ J K}^{-1} \text{ mol}^{-1}$ ), the absolute temperature ( $273 \text{ K}$ ),  
232 the heat of adsorption ( $\text{J mol}^{-1}$ ), and the binding constant ( $\text{L mg}^{-1}$ ), respectively.

233 The Chi-squared ( $\chi^2$ ) test was also used to estimate the fitting of the experimental data to the models'  
234 predicted values. The following equation was used (Arshadi et al., 2014):

235

$$236 \quad \chi^2 = \sum \frac{(Q_e - Q_c)^2}{Q_c}$$

237

238 where  $Q_e$  and  $Q_c$  are the experimental and the model-calculated adsorbed amounts of Cr(VI), respectively.

239

#### 240 **2.4. Kinetics adsorption experiments**

241 Adsorption kinetics experiments were performed to analyze the adsorption mechanism on the surface of  
242 the biochars. Here, an initial concentration of 10 mg L<sup>-1</sup> Cr(VI) was used, while the biochar dose was fixed  
243 at 5 g L<sup>-1</sup>. A relatively low initial Cr(VI) concentration and a comparatively high biochar dose were used  
244 in the kinetics experiments compared with in the equilibrium adsorption experiments to attain maximum  
245 adsorption in the given contact time. Samples with three replicates were placed on a horizontal shaker at  
246 110 rpm, with samples taken at nine different time intervals of 15 min, 30 min, 1 h, 2 h, 3 h, 5 h, 10 h, 24  
247 h, and 48 h. Following this, the samples were filtered through Whatman 42 filter paper and analyzed in  
248 terms of Cr(VI) using the UV-visible spectrophotometer. Different models, including first-order, second-  
249 order, pseudo-second-order, and intra-particle diffusion models were applied to the kinetics experimental  
250 data. The equations of the different models are given below (Ahmad et al., 2013b):

251

252 First-order:  $\ln q_t = \ln q_0 - k_1 t$

253 Second-order:  $\frac{1}{q_t} = \frac{1}{q_0} + k_2 t$

254 Pseudo-second-order:  $\frac{t}{q_t} = \left( \frac{1}{k_2} \frac{1}{q_e^2} \right) + \frac{t}{q_e}$

255 Intra-particle diffusion:  $q_t = C + K_d t^{0.5}$

256

257 where  $q_t$  and  $q_0$  are the adsorption capacities (mg g<sup>-1</sup>) at time  $t$  and 0, respectively,  $k_1$ ,  $k_2$ , and  $k_2'$  are the  
258 rate constants of the first-, second-, and pseudo-second-order models, respectively,  $q_e$  (mg g<sup>-1</sup>) refers to the  
259 adsorption capacity when an equilibrium is established,  $C$  is the diffusion rate constant ([mg g<sup>-1</sup>]<sup>-0.5</sup>), and  
260  $K_d$  is the diffusion constant.

261

## 262 **2.5. Continuous fixed-bed column adsorption and desorption experiments**

263 For the column adsorption experiments, polyacrylic columns 9.4-cm in length and 2-cm in inner diameter  
264 were used. A 7-g sample of each biochar (PBC and EBC) was placed in the polyacrylic columns. The real  
265 wastewater of the tannery industry was passed as an influent through the column from the top at a rate of 6

266 mL min<sup>-1</sup>. The empty bed contact time of the column was 2.83 min. The effluent from each column was  
267 collected from the outlet of the column at different time intervals (0.5, 1, 2, 3, 4, 6, 8, 10, 12, 14, 16, 20,  
268 and 24 h), and was analyzed in terms of Cr(VI) using the UV-visible spectrophotometer. As such, the  
269 effluent samples were continuously analyzed in terms of Cr(VI) until the concentration became almost  
270 equal to the concentration of Cr(VI) in the real wastewater. After exhausting the column with Cr(VI), the  
271 saturated sorbents were eluted with 0.1 N HNO<sub>3</sub> at a flow rate of 6 mL min<sup>-1</sup>.  
272 For the calculations of the adsorption and desorption parameters in the continuous fixed-bed biochar  
273 columns, the methods reported by Zhang et al. (2015) were followed. Details of the column data analysis  
274 for the adsorption and desorption of Cr(VI) are provided in the supplementary material. The behavior of  
275 Cr(VI) adsorption on the two biochars was evaluated by subjecting the experimental column adsorption  
276 data to the Thomas model, which is given by the following equation (Hanbali et al., 2014):

277

$$278 \ln \left[ \frac{C_o}{C_e} - 1 \right] = \frac{k}{Q} [q_m X - C_o V_{ef}]$$

279

280 where  $k$  is the rate constant (mL min<sup>-1</sup> mg<sup>-1</sup>),  $q_m$  is the maximum amount of Cr(VI) adsorbed (mg g<sup>-1</sup>),  $X$  is  
281 the weight of the sorbent (g), and  $V_{ef}$  is the effluent volume (mL). The elution efficiency (E) of each column  
282 was calculated using the following equation:

283

$$284 E (\%) = \left[ \frac{q_{total(desorbed)}}{q_{total(sorbed)}} \right] \times 100$$

285

286 where  $q_{total(desorbed)}$  (mg g<sup>-1</sup>) was calculated from the area under the elution curve.

287

## 288 2.6. Soil remediation experiment

289 The biochars (PBC and EBC) were evaluated in terms of their remediation potential in Cr-contaminated  
290 soil of a specific tannery industry. A soil incubation experiment was conducted using three applications  
291 (1%, 2%, and 5% w/w) of each biochar. Specifically, Cr-contaminated soil (200 g) samples were taken in  
292 each polyethylene container (300-mL capacity) and then mixed with the above-mentioned application rates  
293 for each biochar type. The soil was wetted with 35 mL of distilled water according to 55% of the soil water-  
294 holding capacity. The experiment was conducted in triplicates. Controls (soil without biochar) were also  
295 treated in the same manner. The soil moisture was sustained with distilled water repeatedly throughout the  
296 experiment by weighing each container periodically. The containers were tightly closed and incubated in  
297 the dark at room temperature, with the incubation experiment carried out over 45 days. Following the  
298 incubation, the soil samples of each treatment were air-dried and subjected to various extraction tests to  
299 investigate the bioavailability, leachability, and bioaccessibility of the Cr(VI). The bioavailable Cr(VI) was  
300 measured in a 1:10 soil water extract, while for the toxicity characteristics, the toxicity characteristics  
301 leaching procedure (TCLP) method 1311 (US-EPA, 1992d) was adopted to determine the leachability, with  
302 the bioaccessibility of the Cr(VI) determined following the physiologically based extraction test (PBET)  
303 (Ahmad et al., 2012a). In each extraction test, the filtered extract (using Whatman 42 filter paper) was  
304 analyzed in terms of Cr(VI) via a colorimetric method (as noted earlier).  
305 Water-soluble  $\text{NO}_3$  and  $\text{PO}_4$  (in addition to pH and EC) were also measured in the incubated soils (1:10 soil  
306 water extract) following the colorimetric method while using phenol disulfonic acid and ammonium  
307 molybdate reagents, respectively, with the UV-visible spectrophotometer at 410 and 690 nm, respectively  
308 (Trivedy et al., 1987).

309

## 310 **2.7. Statistical analysis**

311 The mean values of the three replicates were used to plot isotherms for the equilibrium and kinetic  
312 adsorption experiments. Linear and non-linear regressions were carried out in SigmaPlot (version 10.0) for  
313 fitting the adsorption experimental data to various models. Meanwhile, one way analysis of variance was

314 applied in combination with Tukey's honestly significant difference test to determine the significant  
315 differences between the different treatments.

316

### 317 **3. Results and discussion**

#### 318 **3.1. Biochar properties**

319 The results of the proximate and physicochemical analyses of the PBC and the EBC are presented in Table  
320 S2 (supplementary material). The mobile matter in the PBC, which indicates the biodegradable content,  
321 was  $24.11\% \pm 0.56\%$ , which was decreased significantly to  $20.15\% \pm 0.35\%$  in the EBC due to the loss  
322 during the engineering process resulting from, for example, the demineralization with acid (section 2.1;  
323 Vithanage et al., 2015). The ash content in the biochar samples was relatively high ( $>55\%$ ), which could  
324 have been due to the accumulation of inorganic minerals present in the feedstock during the process of  
325 pyrolysis (Ahmad et al., 2014). The PBC was highly alkaline with a pH value of  $9.46 \pm 0.01$ , while the  
326 EBC was slightly acidic with a pH value of  $6.30 \pm 0.01$ . The alkaline nature of the PBC was due to the  
327 existence of alkali salts and the removal of the acidic functional groups during pyrolysis at  $600^{\circ}\text{C}$ .  
328 Meanwhile, the acid demineralization and washing processes during the biochar engineering resulted in the  
329 acidic nature of the EBC. These results were consistent with the EC values of the biochars, where the PBC  
330 had a higher EC ( $0.249 \pm 0.007 \text{ dS m}^{-1}$ ) than the EBC ( $0.149 \pm 0.002 \text{ dS m}^{-1}$ ). Here, the biochar engineering  
331 eliminated one of the limitations of applying alkaline biochars to normal or alkaline soils, as demonstrated  
332 by the EBC, which exhibited an acidic pH. The  $\text{pH}_{\text{PZC}}$  of the PBC and EBC was  $7.44 \pm 0.07$  and  $6.70 \pm$   
333  $0.04$ , respectively, indicating that with any pH lower than this in an aqueous solution, the biochar surfaces  
334 will be positively charged, and vice versa. The organic matter in the PBC ( $1.66\% \pm 0.33\%$ ) was significantly  
335 greater than that in the EBC ( $1.15\% \pm 0.34\%$ ), which was again due to the demineralization step involved  
336 in the engineering process.

337 The surface morphological structures of the biochars were visualized using SEM images (Fig. 1). Here, the  
338 typical plant morphological structure with various pores and channels could be observed in the PBC.  
339 However, the surface structure of the EBC was different from that of the PBC. Here, a relatively smooth

340 surface with diffused pores was observed in the EBC, which was likely due to the engineering with CTAB.  
341 A pore blockage and a decrease in surface area of biochars following CTAB modification have been  
342 previously reported (Liu et al., 2020).

343 The changes in the surface chemistry of the biochars following engineering were analyzed using the FTIR  
344 spectra (Fig. 2), with the spectra interpreted following the information provided by Coates (2000),  
345 Keiluweit et al. (2010), and Li et al. (2018). The FTIR results indicated clear differences in the surface  
346 functional groups of the PBC and the EBC. In the former, the absorbance bands at 1,570, 1,390, 1,024, and  
347  $871\text{ cm}^{-1}$  indicated the presence of C=C-C,  $\text{CH}_2$ , aromatic C-N, and aromatic C-H stretch, respectively.  
348 Specifically, the aromatic C-N and CH out of plane bending vibrations suggested the development of a  
349 stable aromatic structure of the PBC, which was due to the pyrolysis at  $600^\circ\text{C}$ . Meanwhile, more diverse  
350 and intense functional groups were observed in the EBC, which was due to the engineering with CTAB.  
351 Specific bands of the CTAB material were present on the surfaces of the EBC, demonstrating the effect of  
352 modification on the biochar's surface chemistry. The broad band at  $3,290\text{ cm}^{-1}$  indicated the presence of  
353  $\text{NH}_4^+$  ion in the EBC, while the bands at 2,970–2,850, 1,600–1,750, 1,465, 1,280, and  $1,210\text{ cm}^{-1}$  indicated  
354 the typical presence of C-H stretch, carbonyl groups, N- $\text{CH}_3$ , aromatic ether, and C-N groups, respectively.  
355 Meanwhile, the bands at 990–1,100, 890, and  $700\text{ cm}^{-1}$  indicated the presence of P-O-C, Si-O-C, aromatic  
356 C-H stretch, and C-Br, respectively. These results suggested the more complex surface chemistry of the  
357 EBC compared with the PBC.

358 The effect of the engineering process on the biochar properties could further influence their applicability.  
359 In short, the appearance of positively charged ions (e.g.,  $\text{NH}_4^+$ ) on the EBC could facilitate the adsorption  
360 of Cr(VI). Likewise, more acidic functional groups (carbonyl, N- and P-containing functional groups) on  
361 the EBC may contribute to the better removal of anionic Cr(VI) compared with the PBC.

362

### 363 **3.2. Removal of hexavalent chromium from water**

364

#### 365 **3.2.1. Effect of initial hexavalent chromium concentration and contact time**

366 With an increase in initial Cr(VI) concentration (from 5 to 300 mg L<sup>-1</sup>) the removal efficiency of both the  
367 biochars decreased (see Fig. S1a in the supplementary material). This could be due to the occupation of  
368 active sites on the biochar surfaces by the Cr(VI). At high initial Cr(VI) concentrations, fewer active sites  
369 were available to adsorb high contents of Cr(VI). Between the two biochars, the EBC demonstrated a greater  
370 removal efficiency than the PBC. For example, the highest removal efficiency of 79.35% was observed at  
371 a 5-mg L<sup>-1</sup> concentration of Cr(VI) with the EBC, while at the same initial concentration, the PBC  
372 demonstrated only a 37.47% removal. These results indicated that the CTAB engineering may have  
373 increased the number of positively charged active sites on the EBC surface, which subsequently contributed  
374 to its higher removal efficiency compared with that of the PBC. The decrease in removal efficiency with  
375 the elevation in initial metal ion content is a general phenomenon that occurs when testing an adsorbent for  
376 its adsorption capacity (Wadhawan et al., 2020).

377 The contact time between sorbent and sorbate determines the rate of a chemical reaction. Greater adsorption  
378 in a lower time of contact indicates rapid reaction and vice versa. In this study, the results indicated clear  
379 differences between the two biochars in terms of Cr(VI)-removal efficiency, with the EBC demonstrating  
380 greater removal efficiency than the PBC at all contact times. In fact, in the case of the EBC, the Cr(VI)  
381 removal increased from 47.58% to 54.33% within 1.0 h of contact time, followed by a decrease to 48.99%  
382 for 3.0 h and then a gradual increase up to 72.37% after 48 h of contact time. Likewise, there was no sharp  
383 increase in Cr(VI) removal up to 5 h of contact time in the case of the PBC; however, after this point, there  
384 was a gradual increase in Cr(VI) removal up to 42.59% after 48 h of contact time. These results suggest  
385 that both biochars required a longer contact time for the maximum removal of Cr(VI) from water. This  
386 could have been due to the persistence of the natural composition of the feedstock and the limited  
387 availability of active sites, particularly in the case of the PBC. Furthermore, the functional groups on  
388 biochars tend to become stabilized in forming complexes with Cr(VI), thereby lowering the adsorption  
389 efficiency with the increase in contact time (Lian et al., 2019). The pH<sub>PZC</sub> is another important parameter  
390 for determining the charge on biochar surfaces. After 5 h of contact time, the solution pH was lower than  
391 the pH<sub>PZC</sub> of both biochars (solution pH 6.04 < 7.44 pH<sub>PZC</sub> of PBC, and solution pH 6.20 < 6.70 pH<sub>PZC</sub> of

392 EBC), indicating that, at this point, the biochar surfaces were positively charged, which resulted in the  
393 electrostatic attraction of negative ionic species of Cr(VI) ( $\text{Cr}_2\text{O}_7^{2-}$  and  $\text{HCrO}_4^-$ ). However, the biochar  
394 surfaces became negatively charged at and beyond 24 h of contact time when the solution pH was  $> 8$ , thus  
395 causing a slow adsorption rate due to the lack of electrostatic attraction. Nevertheless, the biochar  
396 engineering resulted in comparatively high Cr(VI) removal rates at various time intervals in comparison  
397 with the non-engineered biochar. These results are consistent with those reported by Li et al. (2018), who  
398 described how hydrophilic and hydrophobic functional groups on their CTAB-modified biochar increased  
399 its adsorption efficiency in comparison with the pristine biochar. In the current study, the EBC was loaded  
400 with more aromatic functional groups than the PBC (Fig. 2), which facilitated the greater removal of the  
401 Cr(VI).

402

### 403 3.2.2. Adsorption isotherms

404 The Langmuir, Freundlich, and Temkin isotherm models were fitted through non-linear regressions to the  
405 Cr(VI) adsorption data of the biochars, with the fitting results shown in Fig. 3. Meanwhile, the constant  
406 parameters and  $R^2$  values of the different models for Cr(VI) adsorption onto the different biochars were  
407 obtained and are provided in Table 1a. Here, the  $R^2$  values of the Langmuir model for the PBC and the EBC  
408 were 0.998 and 0.978, respectively, while the corresponding  $\chi^2$  values were 0.073 and 0.700, respectively.  
409 The Langmuir model predicted a maximum adsorption capacity ( $Q_{\text{max}}$ ) of  $14.56 \text{ mg g}^{-1}$  for the PBC and  
410  $27.05 \text{ mg g}^{-1}$  for the EBC. The good fitting of the adsorption data to the Langmuir model indicated that  
411 Cr(VI) may have adsorbed onto the biochar monolayers. Meanwhile, in the Freundlich isotherm model, the  
412  $R^2$  values were 0.986 and 0.964 for the PBC and the EBC, respectively, while the corresponding  $\chi^2$  values  
413 were 0.423 and 1.196, respectively. The constant  $K_F$  is an approximate indicator of adsorption capacity,  
414 while  $N$  is a function of the strength of adsorption in the adsorption process. If the value of  $N$  is below 1, it  
415 indicates normal adsorption, while a value of above 1 indicates cooperative adsorption (Puttamat and  
416 Pavarajarn, 2016). Here, the  $N$  values for both biochars were  $< 1$ , indicating that there was no cooperative  
417 adsorption, while the  $K_F$  value for the EBC ( $0.491 \text{ mg g}^{-1}$ ) was significantly higher than that for the PBC

418 (0.194 mg g<sup>-1</sup>), indicating a similar trend to that of the Langmuir model. Finally, in the Temkin isotherm  
419 model, the R<sup>2</sup> values were 0.914 and 0.818 for the PBC and the EBC, respectively, while the corresponding  
420  $\chi^2$  values were 0.022 and 0.016, respectively. The model-calculated *B* value was lower for the EBC (371.1)  
421 than for the PBC (577.5), indicating the greater adsorption of Cr(VI) onto the EBC due to a decrease in the  
422 adsorption heat and a uniform sharing of the binding energies.

423 Based on the R<sup>2</sup> and  $\chi^2$  values, the Langmuir model was better fitted to our experimental data than the other  
424 models. Somewhat, the EBC demonstrated greater adsorption of Cr(VI) than the PBC, as was predicted by  
425 all three models. It is notable that due to the multivariate properties of biochar, several adsorption  
426 mechanisms could be involved in the elimination of Cr(VI) from water. In this study, the overall controlling  
427 mechanism of adsorption could be the monolayer-to-multilayer adsorption of Cr(VI) onto the biochar  
428 surface, as indicated by the good fit of the adsorption data to both the Langmuir model and the Freundlich  
429 model.

430

### 431 3.2.3. Adsorption kinetics

432 Adsorption kinetics experiments are generally performed to determine the rate of adsorption, including in  
433 terms of mass transport and chemical reaction processes. Here, the adsorption kinetics data were fitted  
434 linearly to various kinetic models (first-order, second-order, pseudo-second-order, and intra-particle  
435 diffusion), as shown in Fig. 4. The calculated constant parameters and R<sup>2</sup> values of the different kinetics  
436 models are given in Table 1b. The pseudo-second-order model exhibited high R<sup>2</sup> values for both the PBC  
437 (0.985) and the EBC (0.996). This model explains that the mechanism of interaction between adsorbent and  
438 adsorbate could be via chemical bonding or via complexation involving electron exchange, which is  
439 generally known as chemisorption. Between the two biochars, the EBC exhibited a greater *q<sub>e</sub>* of 0.851 mg  
440 g<sup>-1</sup> than the PBC (0.497 mg g<sup>-1</sup>), as predicted by the pseudo-second-order model. Similarly, a higher rate  
441 of reaction (*k<sub>2</sub>*) was exhibited by the EBC (1.088 g mg<sup>-1</sup> h<sup>-1</sup>) than the PBC (1.020 g mg<sup>-1</sup> h<sup>-1</sup>), indicating  
442 that the adsorption kinetics of aqueous Cr(VI) occurred faster in the former than in the latter. The other  
443 kinetic models were poorly fitted to the Cr(VI) adsorption data, as indicated by the R<sup>2</sup> values of <0.9. These

444 results indicate that chemisorption could be the main mechanism for aqueous Cr(VI) removal by biochars.  
445 The kinetics analysis also confirmed that the EBC was a more efficient sorbent in removing Cr(VI) from  
446 water.  
447 The adsorption experiments indicated the comparatively greater efficiency of the EBC than the PBC. This  
448 could have been due to the changes in biochar properties following the CTAB engineering. For example,  
449 more aromatic and positively charged functional groups were observed on the EBC than on the PBC (Fig.  
450 2), which could have been involved in complex formation with the Cr(VI). Moreover, the electrostatic  
451 interaction between the highly charged surfaces of the EBC and the Cr(VI) could have resulted in the greater  
452 adsorption efficiency. In fact, the potential role of surface charge in the adsorption of anionic contaminants  
453 with CTAB-modified biochars has previously been reported (Aroke et al., 2014; Mathurasa and  
454 Damrongsiri, 2018).

455

#### 456 **3.2.4. Column adsorption and desorption**

457 The continuous flow fixed-bed columns packed with each PBC and EBC were used for the treatment of  
458 real wastewater contaminated with Cr(VI). The adsorbed amount ( $C_{ad}$ ) of Cr(VI) onto the PBC and EBC  
459 columns as a function of time is shown in Fig. S2a (supplementary material). It was observed that up to 4  
460 h, the  $C_{ad}$  increased gradually, while after this point, the adsorbed amount became almost constant. This  
461 could indicate the equilibrium in Cr(VI) adsorption over time. The saturation time of the fixed-bed column  
462 was relatively short, which could be due to the high flow rate of  $6.0 \text{ mL min}^{-1}$  through the bed of only 6.3  
463 cm height. One of the challenges faced by the column adsorption experiments is the movement of the mass  
464 transfer zone, which is initially saturated with the adsorbate molecules near the bed entrance, and further  
465 restricts the contact of adsorbent with adsorbate, consequently requiring the replacement of the adsorbent  
466 (Patel, 2019). However, as mentioned earlier, this issue can be solved by increasing the bed height of the  
467 column, and increasing the contact time, or decreasing the flow rate of influent into the column. Much like  
468 with the batch adsorption experiments, the EBC demonstrated greater adsorption of Cr(VI) than the PBC.  
469 The performance of the fixed-bed biochar columns in terms of Cr(VI) adsorption was evaluated using the

470 removal percentage of Cr(VI) and the adsorbed amount ( $q_{eq}$ ) onto the biochars in the columns, with the  
471 results presented in Table 2a. The removal efficiencies of the PBC and EBC columns were 60.42% and  
472 74.72%, respectively, while the  $q_{eq}$  values were 18.54 mg/g<sup>-1</sup> and 22.93 mg/g<sup>-1</sup>, respectively. These results  
473 indicated the greater adsorption efficiency of the column packed with the EBC, and were highly consistent  
474 with those of the batch adsorption experiments. The Thomas model parameters and R<sup>2</sup> values are shown in  
475 Table 2b, with the R<sup>2</sup> values found to be 0.462 and 0.667 for the PBC and the EBC, respectively, which  
476 indicated the poor fitting of the column adsorption data to this model. The relatively good fitting of the  
477 Cr(VI) adsorption data for the EBC column to the Thomas model indicated that the adsorption was mainly  
478 through the mass transfer of Cr(VI) onto the EBC. In this study, Cr(VI) was not removed up to 100%, and  
479 the discharge limit of 1.0 mg L<sup>-1</sup> of Cr(VI) in industrial effluent was not achieved, both in the batch and  
480 column adsorption experiments. This could be related to the maximum adsorption potential of the PBC  
481 (14.56 mg g<sup>-1</sup>) and EBC (27.05 mg g<sup>-1</sup>), which restricted the maximum removal of Cr(VI) to around 79%.  
482 However, the removal efficiency can be increased by increasing the amount of adsorbent or bed height of  
483 the column, and increasing the contact time, or decreasing the flow rate of the influent into the column.  
484 Moreover, for practical application, series of fixed-bed adsorption columns can be employed (Patel, 2019).  
485 Once the fixed-bed columns of the PBC and EBC were saturated with Cr(VI), they were eluted with 0.1 M  
486 HNO<sub>3</sub> to desorb the Cr(VI) for the separate measurement of the recovery rate of the PBC and the EBC.  
487 Figure S2b (supplementary material) shows the desorbed concentrations of Cr(VI) from the saturated PBC  
488 and EBC columns at different time intervals. Here, it was observed that at the beginning of the desorption  
489 experiment, the desorbed concentration of Cr(VI) was high in the PBC (20.85 mg L<sup>-1</sup>) and EBC (11.19 mg  
490 L<sup>-1</sup>) columns. The high desorption rate at an initial time, regardless of biochar type, was clear, which was  
491 due to the release of loosely bound Cr(VI) from the biochar surfaces. It was also noted that, initially, the  
492 desorption rate was higher for the PBC column than for the EBC column, indicating that Cr(VI) was more  
493 tightly sorbed onto the EBC. This may suggest some type of strong inner-sphere surface complexation  
494 between the Cr(VI) and the EBC. The total time required for the desorption of Cr(VI) from the columns  
495 was 40 h for the PBC and 44 h for the EBC. In addition, the fitting of the regression lines indicated a more

496 gradual Cr(VI) desorption from the EBC column ( $R^2 = 0.931$ ) than from the PBC column ( $R^2 = 0.813$ ). The  
497 desorbed amount of Cr(VI) and the column elution efficiency for the PBC and EBC are shown in Table 2b.  
498 The total amount of Cr(VI) desorbed from the PBC and EBC packed columns was  $13.83 \text{ mg g}^{-1}$  and  $10.45$   
499  $\text{mg g}^{-1}$ , respectively, with an elution efficiency of 74.61% and 45.56% for the PBC and EBC columns,  
500 respectively. The greater elution efficiency of the PBC suggested that (i) the Cr(VI) was relatively loosely  
501 adsorbed onto the PBC, and (ii) the sorbent could be recycled with greater efficiency after desorbing Cr(VI).  
502 Meanwhile, the comparatively lower elution efficiency of the EBC column suggested that (i) the Cr(VI)  
503 was relatively strongly sorbed onto the EBC, and that (ii) the Cr(VI) adsorption reaction by the EBC was  
504 largely irreversible and that the metal could be retained stably by the EBC. The desorption results indicated  
505 that for the removal of Cr(VI) from wastewater, the PBC could be a good candidate, since it can be reused  
506 in several cycles for this type of removal.

507 A few studies have used peanut-shell-derived biochar, albeit engineered with materials other than CTAB,  
508 for the removal of aqueous Cr(VI). For example, Al-Othman et al. (2012) reported a  $16.26 \text{ mg g}^{-1}$   
509 adsorption capacity of KOH-activated carbon derived from peanut shells, while Wang et al. (2020) reported  
510 a  $15.58 \text{ mg g}^{-1}$  adsorption capacity (at  $20^\circ\text{C}$ ) of kaolinite-modified biochar derived from the same waste  
511 product. Overall, the adsorption performance of the CTAB-engineered biochar in this study in terms of  
512 aqueous Cr(VI) removal ( $27.05 \text{ mg g}^{-1}$ ) was better than those reported in the previous studies.

513

### 514 **3.3. Immobilization of hexavalent chromium in soil**

515 The Cr-contaminated soil was treated with different application rates of the two biochars in an incubation  
516 experiment. The impact of the biochars on the immobilization of Cr(VI) was evaluated by determining the  
517 bioavailable, leachable, and bio-accessible forms of Cr(VI), with the results shown in Fig. 5.

518 The water-soluble fraction of metals is considered to be the most bioavailable form in soil, one that is  
519 readily available for plant uptake. Here, the biochar treatments significantly decreased the water-soluble  
520 Cr(VI) content compared with that in the control (Fig. 5a). Specifically, at 1%, 2% and 5% (wt/wt) of the  
521 PBC application rates, the water-soluble Cr(VI) decreased from  $40.65 \text{ mg kg}^{-1}$  (in control soil) to 28.86,

522 23.52, and 13.33 mg kg<sup>-1</sup>, respectively. Meanwhile, at 1%, 2% and 5% (wt/wt) applications, the EBC  
523 decreased the water-soluble Cr(VI) content to 20.28, 8.14, and 3.35 mg kg<sup>-1</sup>, respectively. These results  
524 indicated the enhanced immobilization of Cr(VI) in the soil with an increase in biochar application rate. On  
525 comparing the two biochars at the respective applications, the EBC demonstrated a greater decrease in  
526 bioavailability of Cr(VI) (up to 91.75%) in the soil. The possible reason for the greater immobilization  
527 efficiency of EBC was related to the reduction of Cr(VI) through the carbonyl functional groups acting as  
528 proton donors (Mandal et al., 2017).

529 The TCLP test is recommended for determining the toxicity of metals in soil, particularly in terms of metals  
530 leaching from the soil to the groundwater as a result of acid rain. The control soil with no biochar exhibited  
531 high TCLP Cr(VI) content (101.74 mg kg<sup>-1</sup>; Fig. 5b), indicating that the soil was highly susceptible to  
532 Cr(VI) leaching into the groundwater, ultimately causing toxicity. The greater TCLP Cr(VI) content in  
533 relation to water-soluble Cr(VI) was due to the acidic extractant (acetic acid) used in the TCLP test. The  
534 leachability of Cr(VI) was significantly decreased by the biochars at different applications. Meanwhile, the  
535 increase in biochar application resulted in an increase in the immobilization of Cr(VI) in the soil, which  
536 could ultimately decrease the toxicity of groundwater. Much like the bioavailable Cr(VI), the leachable  
537 Cr(VI) fraction was reduced at a greater rate by the EBC (up to 100%) than the PBC (up to 82.01%). These  
538 results suggest that the binding interaction of the EBC in terms of Cr(VI) was greater than that of the PBC.  
539 To ascertain the impact of biochars on the direct ingestion of Cr(VI)-contaminated soil by mammals, a  
540 PBET test was performed. This test is useful for determining the toxicity of metals during soil ingestion in  
541 the stomach of mammals since the extractant used is highly acidic and is thus representative of actual  
542 stomach conditions. The results of the PBET test for Cr(VI) concentration in the contaminated soil treated  
543 with the biochars are shown in Fig. 5c. Here, the control soil with no biochar exhibited the highest PBET  
544 Cr(VI) concentration (168.97 mg kg<sup>-1</sup>), which was likely due to the high acidic conditions employed in the  
545 PBET test. Both the biochars achieved a significant decrease in the bioaccessibility of Cr(VI), while an  
546 increase in biochar application resulted in a greater decrease in the bio-accessible fraction of Cr(VI).  
547 Between the two biochars, the EBC again demonstrated a greater immobilization of Cr(VI) (up to 97.26%)

548 in soil than the PBC (up to 73.32%). These results are consistent with the bioavailable and leachable  
549 fractions of Cr(VI).

550 Overall, in terms of the remediation of Cr-contaminated soil, both biochars were effective in immobilizing  
551 the Cr(VI), thereby decreasing its potential to cause toxicity. The greater immobilization effect of the EBC  
552 than the PBC indicated that a strong chemical interaction between the Cr(VI) and the EBC surface could  
553 have been present. The Cr(VI) remediation in contaminated soil was in good agreement with the results for  
554 the Cr(VI) removal from water. Compared with the few available studies on Cr(VI) immobilization in soil  
555 using modified biochars, we reported a good efficiency of the EBC. For example, Zibaei et al. (2020)  
556 reported 46.23% and 38.95% reductions of Cr(VI) in soil with chitosan-modified and hematite-modified  
557 biochars, respectively, while Mandal et al. (2017) reported 55% and 48% reductions in Cr(VI) with chitosan  
558 + zerovalent iron-modified sheep manure and poultry-manure-derived biochars, respectively, and Wang et  
559 al. (2019) observed a 67.34% decrease in the bioavailability of Cr(VI) in soil treated with bacteria-modified  
560 biochar.

561 Other soil parameters, such as pH, EC, soluble-NO<sub>3</sub>, and PO<sub>4</sub>, were also analyzed to evaluate the effect of  
562 biochars on soil quality, with the results shown in Fig. S3 (supplementary material). A significant increase  
563 in the pH was observed for the soils amended with the biochars (Fig. S3a). However, the soil pH was <8,  
564 indicating no harmful impact of the biochars since plants can grow normally in such soil types (Soti et al.,  
565 2015). A significant decrease in the EC value of the soil was observed in all the biochar applications in  
566 relation to the control (Fig. S3b). The reason for this decrease in soil EC could be attributed to the retention  
567 of dissolved ions (e.g., Ca<sup>2+</sup>) on the empty exchange sites of the biochar (Sultan et al., 2020). Specifically,  
568 the 5% application of the EBC significantly decreased the soil EC (0.02 dS m<sup>-1</sup>), which could have been  
569 due to its higher adsorption efficiency in terms of soluble ions than the PBC (0.07 dS m<sup>-1</sup>), as was  
570 ascertained from the adsorption experiments. Meanwhile, the soils amended with the PBC exhibited a  
571 considerable decrease in the water-soluble NO<sub>3</sub> and PO<sub>4</sub> concentrations (Fig. S3c, d), with the increased  
572 application of PBC demonstrating the maximum NO<sub>3</sub> and PO<sub>4</sub> adsorption. In fact, the NO<sub>3</sub> and PO<sub>4</sub>  
573 adsorption onto biochars has previously been reported (Zhou et al., 2019). In contrast, the EBC exhibited a

574 significant increase in the  $\text{NO}_3$  and  $\text{PO}_4$  concentrations (especially at 1% and 2% applications) compared  
575 with the control. This could be attributed to the N- and P-containing functional groups present on the EBC  
576 surfaces (Fig. 2). From these results, it can be inferred that the EBC could enhance the soil fertility by  
577 increasing the bioavailable  $\text{NO}_3$  and  $\text{PO}_4$  contents in the soil, subsequently improving the plant's growth if  
578 the soil is used for agricultural purposes.

579 Given the better performance of engineered biochar than its pristine counterpart in remediating Cr-  
580 contaminated water and soil, and given the additional engineering steps required, the cost of this novel  
581 approach could be high (not calculated in this study). However, the benefits of the engineered biochar in  
582 comparison with the pristine biochar in terms of higher remediation efficiency could make it an attractive  
583 approach in the future. In short, we can design biochars in accordance with the desired application through  
584 engineering to avoid any negative impact. Furthermore, using cheap alternative resources, such as  
585 household commodities and waste, for the production of engineered biochar could reduce the cost of the  
586 attendant technology and subsequently increase the economic profitability.

587

#### 588 **4. Conclusions**

589 The equilibrium adsorption isotherm experiments indicated a greater adsorption capacity of the engineered  
590 biochar (modified with CTAB) than the pristine biochar (derived from peanut shell). The Langmuir model  
591 adequately described the adsorption of Cr(VI) onto the biochars, indicating a monolayer type adsorption  
592 process. The application of specific kinetic models indicated that chemisorption was the dominant  
593 mechanism governing the interaction of Cr(VI) with the pristine and engineered biochars. Similarly, Cr(VI)  
594 adsorption decreased gradually through continuous flow fixed-bed columns packed with the pristine and  
595 engineered biochars, while the column desorption experiments indicated that Cr(VI) was more tightly  
596 adsorbed onto the engineered biochar, suggesting a strong inner-sphere complexation between Cr(VI) and  
597 this biochar. To meet the standard discharge limit ( $1.0 \text{ mg L}^{-1}$ ) of Cr(VI) from industrial effluents, it is  
598 recommended to consider increased bed height, slow flow rate, and series of fixed-bed columns. Both the  
599 biochars also demonstrated a great reduction in the bioavailability, leachability, and bioaccessibility of

600 Cr(IV) in soil. Much like with the water remediation, the engineered biochar was more effective in  
601 immobilizing Cr(VI) in the soil. Furthermore, the engineered biochar increased the water-soluble nitrate  
602 and phosphate in the amended soil in comparison with the unamended soil, indicating that the remediated  
603 soil could be utilized for agricultural purposes. For future research, we suggest employing other engineering  
604 processes such as impregnation/coating with chemicals to increase the positive surface charge on biochar  
605 for more efficient removal of Cr(VI) from tannery wastewater. Before practical application of the new  
606 adsorption technology, the associated factors affecting the removal efficiency, and the permissible  
607 discharge limit of the pollutant should be considered.

608

#### 609 **Acknowledgment**

610 The study was partly supported by the University Research Fund (URF).

611

#### 612 **References**

613 Ahmad, M., Lee, S.S., Dou, X., Mohan, D., Sung, J.K., Yang, J.E., Ok, Y.S., 2012a Effects of pyrolysis  
614 temperature on soybean stover- and peanut shell-derived biochar properties and TCE adsorption in  
615 water. *Bioresour. Technol.*, 118, 536-544.

616 Ahmad, M., Lee, S.S., Yang, J.E., Ro, H.M., Lee, Y.H., Ok, Y.S., 2012b Effects of soil dilution and  
617 amendments (musselshell, cowbone, and biochar) on Pb availability and phytotoxicity in military  
618 shooting range soil. *Ecotoxicol. Environ. Saf.*, 79, 225-231.

619 Ahmad, M., Lee, S.S., Rajapaksha, A.U., Vithanage, M., Zhang, M., Cho, J.K., Lee, S.E., Ok, Y.S., 2013a  
620 Trichloroethylene adsorption by pine needle biochars produced at various pyrolysis temperatures.  
621 *Bioresour. Technol.*, 143, 615-622.

622 Ahmad, M., Lee, S.S., Oh, S.E., Mohan, D., Moon, D.H., Lee, Y.H., Ok, Y.S., 2013b Modeling adsorption  
623 kinetics of trichloroethylene onto biochars derived from soybean stover and peanut shell wastes.  
624 *Environ. Sci. Pollut. Res.*, 20, 8364-8373.

625 Ahmad, M., Rajapaksha, A.U., Lim, J.E., Zhang, M., Bolan, N., Mohan, D., Vithanage, M., Lee, S.S., Ok,  
626 Y.S., 2014 Biochar as a sorbent for contaminant management in soil and water: A review.  
627 Chemosphere, 99, 19-33.

628 Al-Othman, Z.A., Ali, R., Naushad, M., 2012 Hexavalent chromium removal from aqueous medium by  
629 activated carbon prepared from peanut shell: Adsorption kinetics, equilibrium and thermodynamic  
630 studies. Chem. Eng. J., 184, 238-247.

631 Aroke, U.O., El-Nafaty, U.A., Osha, O.A., 2014 Removal of oxyanion contaminants from wastewater by  
632 sorption on to HDTMA Br surface modified organo kaolinite clay. Int. J. Emerging Technol. Adv.  
633 Eng., 4, 475-484.

634 Arshadi, M., Amiri, M.J., Mousavi, S., 2014 Kinetic, equilibrium and thermodynamic investigations of  
635 Ni(II), Cd(II), Cu(II) and Co(II) adsorption on barley straw ash. Water Resour. Ind., 6, 1-17.

636 Bhalli, J.A., Khan, Q.M., 2006 Pollution level analysis in tannery effluents collected from three different  
637 cities of Punjab, Pakistan. Pak. J. Biol. Sci., 9, 418-421.

638 Chilton, P.J., Jamieson, D., Abid, M.S., Milne, C.J., Ince, M.E., Aziz, J.A., 2001 Pakistan water quality  
639 mapping and management project. Pakistan Integrated Household Survey (PIHS) Islamabad, Federal  
640 Bureau of Statistics, Government of Pakistan.

641 Coates, J., 2000 Interpretation of Infrared Spectra, a Practical Approach. In: Meyers, R.A. (Ed.),  
642 Encyclopedia of Analytical Chemistry. John Wiley & Sons Ltd, Chichester, pp. 10815–10837.

643 Duc, P.A., Dharanipriya, P., Velmurugan, B.K., Shanmugavadivu, M., 2019 Groundnut shell -a beneficial  
644 bio-waste. Biocatal. Agric. Biotechnol., 20, 101206.

645 El-Naggar, A., Shaheen, S.M., Ok, Y.S., Rinklebe, J., 2018a Biochar affects the dissolved and colloidal  
646 concentrations of Cd, Cu, Ni, and Zn and their phytoavailability and potential mobility in a mining soil  
647 under dynamic redox-conditions. Sci. Total Environ., 624, 1059-1071.

648 El-Naggar, A., Lee, S.S., Awad, Y.M., Yang, X., Ryu, C., Rizwan, M., Rinklebe, J., Tsang, D.C.W., Ok,  
649 Y.S., 2018b Influence of soil properties and feedstocks on biochar potential for carbon mineralization  
650 and improvement of infertile soils. Geoderma, 332, 100-108.

651 Estefan, G., Sommer, R., Ryan, J., 2013 *Methods of Soil, Plant, and Water Analysis: A manual for the West*  
652 *Asia and North Africa region*. 3<sup>rd</sup> ed. ICARDA (International Center for Agricultural Research in the  
653 *Dry Areas*) Box 114/5055, Beirut, Lebanon, pp. 243.

654 Fytianos, K., Voudrias, E., Kokkalis, E., 2000 Sorption–desorption behaviour of 2, 4-dichlorophenol by  
655 *marine sediments*. *Chemosphere*, 40, 3-6.

656 Hanbali, M., Holail, H., Hammud, H., 2014 Remediation of lead by pretreated red algae: adsorption  
657 *isotherm, kinetic, column modeling and simulation studies*. *Green Chem. Lett. Rev.*, 7, 342-358.

658 Hilber, I., Bucheli, T.D., 2010 Activated carbon amendment to remediate contaminated sediments and soils:  
659 *A review*. *Global Nest J.*, 12, 305-317.

660 Huang, S.W., Chen, X., Wang, D.D., Jia, H.L., Wu, L., 2020 Bio-reduction and synchronous removal of  
661 *hexavalent chromium from aqueous solutions using novel microbial cell/algal-derived biochar*  
662 *particles: Turning an environmental problem into an opportunity*. *Bioresour. Technol.*, 309, 123304.

663 Jobby, R., Jha, P., Yadav, A.K., Desai, N. 2018 Biosorption and biotransformation of hexavalent chromium  
664 *[Cr(VI)]: A comprehensive review*. *Chemosphere* 207, 255-266.

665 Keiluweit, M., Nico, P.S., Johnson, M.G., Kleber, M., 2010 Dynamic molecular structure of plant biomass-  
666 *derived black carbon (biochar)*. *Environ. Sci. Technol.*, 44, 1247-1253.

667 Khan, A.Z., Khan, S., Ayaz, T., Brusseau, M.L., Khan, M.A., Nawab, J., Muhammad, S., 2020 Popular  
668 *wood and sugarcane bagasse biochars reduced uptake of chromium and lead by lettuce from mine-*  
669 *contaminated soil*. *Environ. Pollut.*, 263, 114446.

670 Kumar, A., Bhattacharya, T., 2020 Biochar: a sustainable solution. *Environ. Dev. Sustain.*,  
671 <https://doi.org/10.1007/s10668-020-00970-0>

672 Kumar, R., Devanathan, A., Rai, A.K., 2015 Speciation of Cr(III) and Cr(VI) in industrial wastewater using  
673 *biphasic extraction and determination by LIBS*. *J. Found. Appl. Phys.*, 2, 61-70.

674 Li, H., Dong, X., da Silva, E.B., de Oliveira, L.M., Chen, Y., Ma, L.Q., 2017 Mechanisms of metal sorption  
675 *by biochars: Biochar characteristics and modifications*. *Chemosphere*, 178, 466-478.

676 Li, Y., Wei, Y., Huang, S., Liu, X., Jin, Z., Zhang, M., Qu, J., Jin, Y., 2018 Biosorption of Cr(VI) onto  
677 *Auricularia auricula* dreg biochar modified by cationic surfactant: Characteristics and mechanism. J.  
678 Mol. Liq., 269, 824-832.

679 Lian, G., Wang, B., Lee, X., Li, L., Liu, T., Lyu, W., 2019 Enhanced removal of hexavalent chromium by  
680 engineered biochar composite fabricated from phosphogypsum and distillers grains. Sci. Total  
681 Environ., 697, 134119.

682 Liu, W., Ren, D., Wu, J., Wang, Z., Zhang, S., Zhang, X., Gong, X., 2020 Adsorption behavior of 2,4-DCP  
683 by rice straw biochar modified with CTAB. Environ. Technol.,  
684 <https://doi.org/10.1080/09593330.2020.1743367>

685 Mandal, S., Sarkar, B., Bolan, N., Ok, Y.S., Naidu, R., 2017 Enhancement of chromate reduction in soils  
686 by surface modified biochar. J. Environ. Manage., 186, 277-284.

687 Mathurasa, L., Damrongsiri, S., 2017 Potential of using surfactants to enhance ammonium and nitrate  
688 adsorption on rice husk and its biochar. Appl. Environ. Res. 39, 11-22.

689 Mathurasa, L., Damrongsiri, S., 2018 Low cost and easy rice husk modification to efficiently enhance  
690 ammonium and nitrate adsorption. Int. J. Recycl. Org. Waste Agric., 7, 143-151.

691 Mehmood, K., Ahmad, H.R., Saifullah, 2019 Quantitative assessment of human health risk posed with  
692 chromium in waste, ground, and surface water in an industrial hub of Pakistan. Arab. J. Geosci., 12,  
693 283.

694 Mi, X., Li, G., Zhu, W., Liu, L., 2016 Enhanced adsorption of orange II using cationic surfactant modified  
695 biochar pyrolyzed from cornstalk. J. Chem., 2016, Article ID 8457030, 7.

696 Mohan, D., Pittman, Jr., 2006 Activated carbons and low cost adsorbents for remediation of tri- and  
697 hexavalent chromium from water. J. Hazard. Mater., B137, 762-811.

698 Palansooriya, K.M., Shaheen, S.M., Chen, S.S., Tsang, D.C.W., Hashimoto, Y., Hou, D., Bolan, N.S.,  
699 Rinklebe, J., 2020 Soil amendments for immobilization of potentially toxic elements in contaminated  
700 soils: A critical review. Environ. Int., 134, 105046.

701 PARC, 2020 Pakistan Agricultural Research Council. [http://www.parc.gov.pk/index.php/en/csi/137-](http://www.parc.gov.pk/index.php/en/csi/137-narc/crop-sciences-institute/728-groundnut)  
702 [narc/crop-sciences-institute/728-groundnut](http://www.parc.gov.pk/index.php/en/csi/137-narc/crop-sciences-institute/728-groundnut)

703 Patel, H., 2019 Fixed-bed column adsorption study: a comprehensive review. *Appl. Water Sci.*, 9, 45.

704 Puttamat, S., Pavarajarn, V., 2016 Adsorption study for removal of Mn(II) ion in aqueous solution by  
705 hydrated ferric(III) oxides. *Int. J. Chem. Eng. Appl.*, 7, 239-243.

706 Qadir, A., Malik, R.N., Husain, S.Z., 2008 Spatio-temporal variations in water quality of Nullah Aik-  
707 tributary of the river Chenab, Pakistan. *Environ. Monit. Assess.*, 140, 43-59.

708 Rafique, M.I., Usman, A.R.A., Ahmad, M., Sallam, A., Al-Wabel, M.I., 2020 In situ immobilization of Cr  
709 and its availability to maize plants in tannery waste-contaminated soil: effects of biochar feedstock  
710 and pyrolysis temperature. *J. Soils Sediments*, 20, 330-339.

711 Rajapaksha, A.U., Alam, M.S., Chen, N., Alessi, D.S., Igalavithana, A.D., Tsang, D.C.W., Ok, Y.S., 2018  
712 Removal of hexavalent chromium in aqueous solutions using biochar: Chemical and spectroscopic  
713 investigations. *Sci. Total Environ.*, 625, 1567-1573.

714 Rajapaksha, A.U., Chen, S.S., Tsang, D.C.W., Zhang, M., Vithanage, M., Mandal, S., Gao, B., Bolan, N.S.,  
715 Ok, Y.S., 2016 Engineered/designer biochar for contaminant removal/immobilization from soil and  
716 water: Potential and implication of biochar modification. *Chemosphere*, 148, 276-291.

717 Rehman, S., Adnan, M., Iqbal, M., Nafees, M., 2017 Working efficiency of waste water treatment facility  
718 in Hayatabad industrial estates, Peshawar. *J. Sci. Technol.*, 40, 41-52.

719 Riaz, U., Murtaza, G., Saifullah, Farooq, M., Aziz, H., Qasir, A.A., Mehdi, S.M., Qazi, M.A., 2020  
720 Chemical fractionation and risk assessment of trace elements in sewage sludge generated from various  
721 states of Pakistan. *Environ. Sci. Pollut. Res.*, <https://doi.org/10.1007/s11356-020-07795-4>

722 Sabur, M.A., Rahman, M.M., Safiullah, S., 2013 Treatment of tannery effluent by locally available  
723 commercial grade lime. *J. Sci. Res.* 5, 143-150.

724 Saleh, M.M., 2006 On the removal of cationic surfactants from dilute streams by granular charcoal. *Water*  
725 *Res.*, 40, 1052-1060.

726 Soti, P.G., Jayachandran, K., Koptur, S., Volin, J.C., 2015 Effect of soil pH on growth, nutrient uptake, and  
727 mycorrhizal colonization in exotic invasive *Lygodium microphyllum*. *Plant Ecol.*, 216, 989-998.

728 Sultan, H., Ahmed, N., Mubashir, M., Danish, S., 2020 Chemical production of acidified activated carbon  
729 and its influences on soil fertility comparative to thermo-pyrolyzed biochar. *Sci. Rep.*, 10, 595.  
730 <https://doi.org/10.1038/s41598-020-57535-4>

731 Tan, C., Zeyu, Z., Sai, X., Hongtao, W., Wenjing, L., 2015 Adsorption behavior comparison of trivalent  
732 and hexavalent chromium on biochar derived from municipal sludge. *Bioresour. Technol.*, 190, 388-  
733 394.

734 Torkashvand, A.M., Alidoust, M., Khomami, A.M., 2015 The reuse of peanut organic wastes as a growth  
735 medium for ornamental plants. *Int. J. Recycl. Org. Waste Agricult.*, 4, 85-94.

736 Tran, H.N., You, S.J., Bandegharai, A.H., Chao, H.P., 2017 Mistakes and inconsistencies regarding  
737 adsorption of contaminants from aqueous solutions: A critical review. *Water Res.*, 120, 88-116.

738 Trivedy, R.K., Goel, P.K., Trisal, C.L., 1987 Practical methods in ecology and environmental science.  
739 Enviro Media Publications, pp 340.

740 US-EPA, 1992a Method 3005a Acid digestion of waters for total recoverable or dissolved metals for  
741 analysis by FLAA or ICP spectroscopy. United States Environmental Protection Agency.

742 US-EPA, 1992b Method 7196a Chromium, hexavalent (colorimetric). United States Environmental  
743 Protection Agency.

744 US-EPA, 1992c Method 3050 Acid digestion of sediments, sludges, and soils. United States Environmental  
745 Protection Agency.

746 US-EPA, 1992d Method 1311 Toxicity characteristic leaching procedure. United States Environmental  
747 Protection Agency.

748 US-EPA, 2014 Priority Pollutant List. United States Environmental Protection Agency.

749 Vithanage, M., Rajapaksha, A.U., Zhang, M., Thiele-Bruhn, S., Lee, S.S., Ok, Y.S., 2015 Acid-activated  
750 biochar increased sulfamethazine retention in soils. *Environ. Sci. Pollut. Res.*, 22, 2175-2186.

751 Volesky, B., 2007 Biosorption and me. *Water Res.*, 41, 4017-4029.

752 Wadhawan, S., Jain, A., Nayyar, J., Mehta, S.K., 2020 Role of nanomaterials as adsorbents in heavy metal  
753 ion removal from waste water: A review. *J. Water Process Eng.*, 33, 101038.

754 Wang, C., Gu, L., Ge, S., Liu, X., Zhang, X., Chen, X., 2019 Remediation potential of immobilized bacterial  
755 consortium with biochar as carrier in pyrene-Cr(VI) co-contaminated soil. *Environ. Technol.*, 40,  
756 2345-2353.

757 Wang, H., Yang, N., Qiu, M., 2020 Adsorption of Cr(VI) from aqueous solution by biochar-clay derived  
758 from clay and peanut shell. *J. Inorg. Mater.*, 35, 301-308.

759 Wang, L., Cho, D.W., Tsang, D.C.W., Cao, X., Hou, D., Shen, Z., Alessi, D.S., Ok, Y.S., Poon, C.S., 2019  
760 Green remediation of As and Pb contaminated soil using cement-free clay-based  
761 stabilization/solidification. *Environ. Int.*, 126, 336-345.

762 Wang, L., Ok, Y.S., Tsang, D.C.W., Alessi, D.S., Rinklebe, J., Wang, H., Masek, O., Hou, R., O'Connor,  
763 D., Hou, D., 2020 New trends in biochar pyrolysis and modification strategies: feedstock, pyrolysis  
764 conditions, sustainability concerns and implications for soil amendment. *Soil Use Manag.*, 36, 358-  
765 386.

766 WHO. 2000. Global water supply and sanitation assessment 2000 report. World Health Organization.

767 Xia, S., Song, Z., Jeyakumar, P., Shaheen, S.M., Rinklebe, J., Ok, Y.S., Bolan, N., Wang, H., 2019 A  
768 critical review on bioremediation technologies for Cr(VI)-contaminated soils and wastewater. *Crit.*  
769 *Rev. Env. Sci.*, 49, 1027-1078.

770 Xu, D., Gao, Y., Lin, Z., Gao, W., Zhang, H., Karnowo, K., Hu, X., Sun, H., Hassan, S.S.A.S., Zhang, S.,  
771 2019 Application of biochar derived from pyrolysis of waste fiberboard on tetracycline adsorption in  
772 aqueous solution. *Front. Chem.*, 7:943. doi: 10.3389/fchem.2019.00943

773 Yang, X., Wan, Y., Zheng, Y., He, F., Yu, Z., Huang, J., Wang, H., Ok, Y.S., Jiang, Y., Gao, B., 2019  
774 Surface functional groups of carbon-based adsorbents and their roles in the removal of heavy metals  
775 from aqueous solutions: A critical review. *Chem. Eng. J.*, 366, 608-621.

776 Zhang, A., Li, X., Xing, J., Xu, G., 2020 Adsorption of potentially toxic elements in water by modified  
777 biochar: A review. *J. Environ. Chem. Eng.*, 8, 104196.

778 Zhang, M., Ahmad, M., Al-Wabel, M.I., Vithanage, M., Rajapaksha, A.U., Kim, H.S., Lee, S.S., Ok, Y.S.,  
779 2015 Adsorptive removal of trichloroethylene in water by crop residue biochars pyrolyzed at  
780 contrasting temperatures: continuous fixed-bed experiments. J. Chem. 2015. Article ID 647072, 6.

781 Zhou, L., Xu, D., Li, Y., Pan, Q., Wang, J., Xue, L., Howard, A., 2019 Phosphorus and nitrogen  
782 adsorption capacities of biochars derived from feedstocks at different pyrolysis temperatures. Water,  
783 2019, 11, 1559.

784 Zibaei, Z., Fasaee, R.G., Ronaghi, A., Zarei, M., Zeinali, S., Improvement of biochar capability in Cr  
785 immobilization via modification with chitosan and hematite and inoculation with *Pseudomonas*  
786 *putida*. Commun. Soil Sci. Plant Anal., 51, 963-975.

787

788

789 **List of Tables**

790 **Table 1:** Parameters of different adsorption isotherm models (a) and kinetic models (b) for the removal of  
791 Cr(VI) from water by the PBC and the EBC.

792 **Table 2:** (a) Adsorption process parameters and Thomas model parameters for Cr(VI) adsorption, and (b)  
793 desorption process parameters for Cr(VI) desorption for the PBC and the EBC in continuous fixed-  
794 bed columns.

795

796

797

798

799

800

801

802

803

804

805

806

807

808

809

810

811

812

813

814

815 **List of Figures**

816 **Fig. 1:** The SEM images of (a) the pristine biochar (PBC) and (b) the engineered biochar (EBC).

817 **Fig. 2:** The FTIR spectra of (a) the pristine biochar (PBC) and (b) the engineered biochar (EBC).

818 **Fig. 3:** Non-linear fittings of the (a) Langmuir, (b) Freundlich, and (c) Temkin isotherm models to the  
819 experimental data of Cr(VI) adsorption onto the pristine biochar (PBC) and the engineered biochar  
820 (EBC).

821 **Fig. 4:** Linear fittings of the (a) first-order, (b) second-order, (c) pseudo-second order, and (d) intra-particle  
822 diffusion kinetic models to the experimental data of Cr(VI) adsorption onto the pristine biochar  
823 (PBC) and the engineered biochar (EBC).

824 **Fig. 5:** Effect of various application rates of the pristine biochar (PBC) and the engineered biochar (EBC)  
825 on (a) water, (b) TCLP, and (c) PBET extracted Cr(VI) in contaminated soil. The similar letters on  
826 each bar indicate non-significant differences between the different treatments at  $P < 0.05$  (\* = not  
827 detected).

828

829 **Table 1:** Parameters of different adsorption isotherm models (a) and kinetic models (b) for the removal of Cr(VI) from water by the pristine biochar  
 830 (PBC) and the engineered biochar (EBC).

831 **(a)**

Biochar/ isotherm model	Langmuir				Freundlich				Temkin			
	R <sup>2</sup>	χ <sup>2</sup>	Q <sub>max</sub> (mg g <sup>-1</sup> )	K <sub>L</sub> (L g <sup>-1</sup> )	R <sup>2</sup>	χ <sup>2</sup>	N	K <sub>F</sub> (mg g <sup>-1</sup> )	R <sup>2</sup>	χ <sup>2</sup>	B	A
PBC	0.998	0.073	14.56	0.006	0.986	0.423	0.699	0.194	0.914	0.200	577.5	0.181
EBC	0.978	0.700	27.05	0.009	0.964	1.196	0.696	0.491	0.818	0.519	371.1	0.403

831

832 **(b)**

Biochar/ kinetic model	First order			Second order			Pseudo-second order				Intra-particle diffusion				
	R <sup>2</sup>	χ <sup>2</sup>	k <sub>1</sub> (g mg <sup>-1</sup> h <sup>-1</sup> )	R <sup>2</sup>	χ <sup>2</sup>	k <sub>2</sub> (g mg <sup>-1</sup> h <sup>-1</sup> )	R <sup>2</sup>	χ <sup>2</sup>	q <sub>e</sub> (mg g <sup>-1</sup> )	k <sub>2</sub> ' (g mg <sup>-1</sup> h <sup>-1</sup> )	h (mg g <sup>-1</sup> h <sup>-1</sup> )	R <sup>2</sup>	χ <sup>2</sup>	K <sub>d</sub> (mg g <sup>-1</sup> )	C
PBC	0.891	0.031	0.011	0.859	0.104	-0.030	0.985	10.351	0.497	1.020	0.252	0.835	0.022	0.031	0.261
EBC	0.836	0.089	0.008	0.810	0.047	-0.012	0.996	2.360	0.851	1.088	0.788	0.877	0.016	0.045	0.542

833 **Table 2:** (a) Adsorption process parameters and Thomas model parameters for Cr(VI) adsorption and (b)  
 834 desorption process parameters for Cr(VI) desorption for the pristine biochar (PBC) and the engineered  
 835 biochar (EBC) in continuous fixed-bed columns.

**(a)**

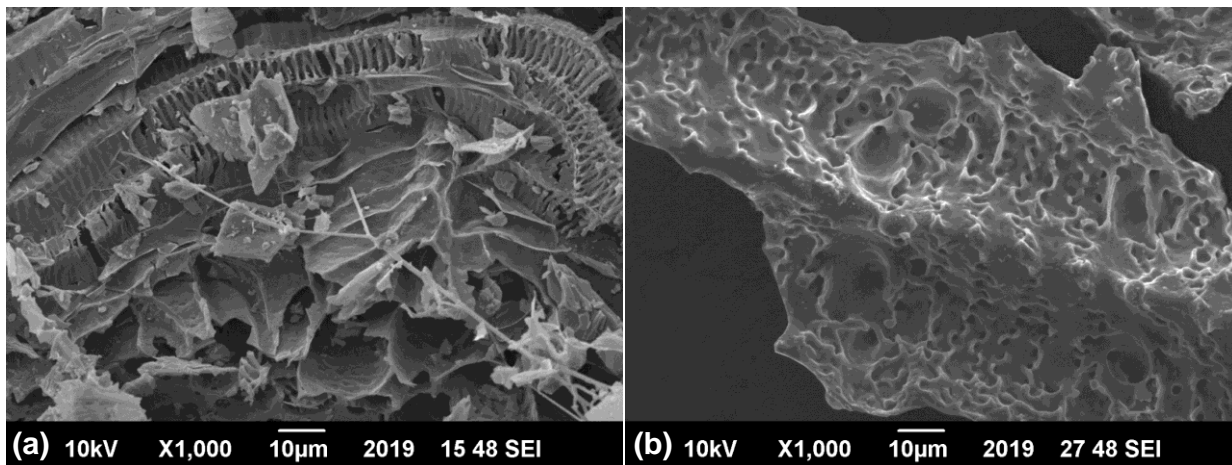
Biochar	Sorption process		Thomas model		
	Removal	$q_{eq}$	$k$	$q_0$	$R^2$
	(%)	( $mg\ g^{-1}$ )	( $mL\ min^{-1}\ mg^{-1}$ )	( $mg\ g^{-1}$ )	
PBC	60.42	18.54	0.048	3.28	0.462
EBC	74.72	22.93	0.072	2.03	0.667

**(b)**

Biochar	Desorbed Cr(VI)	Column elution efficiency
	( $mg\ g^{-1}$ )	(%)
PBC	13.83	74.61
EBC	10.45	45.56

836

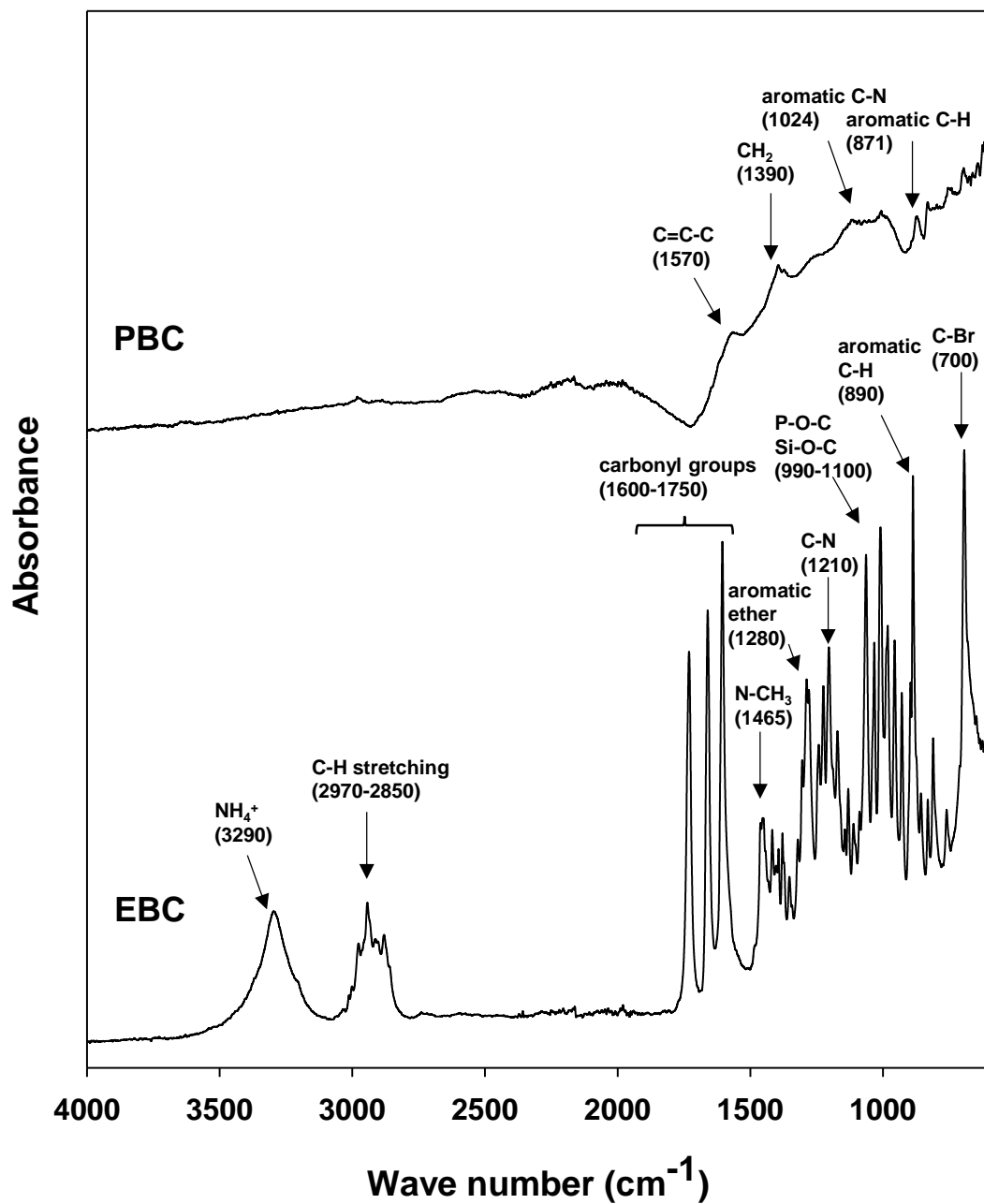
837



838

839 **Fig. 1:** The SEM images of (a) the pristine biochar (PBC) and (b) the engineered biochar (EBC).

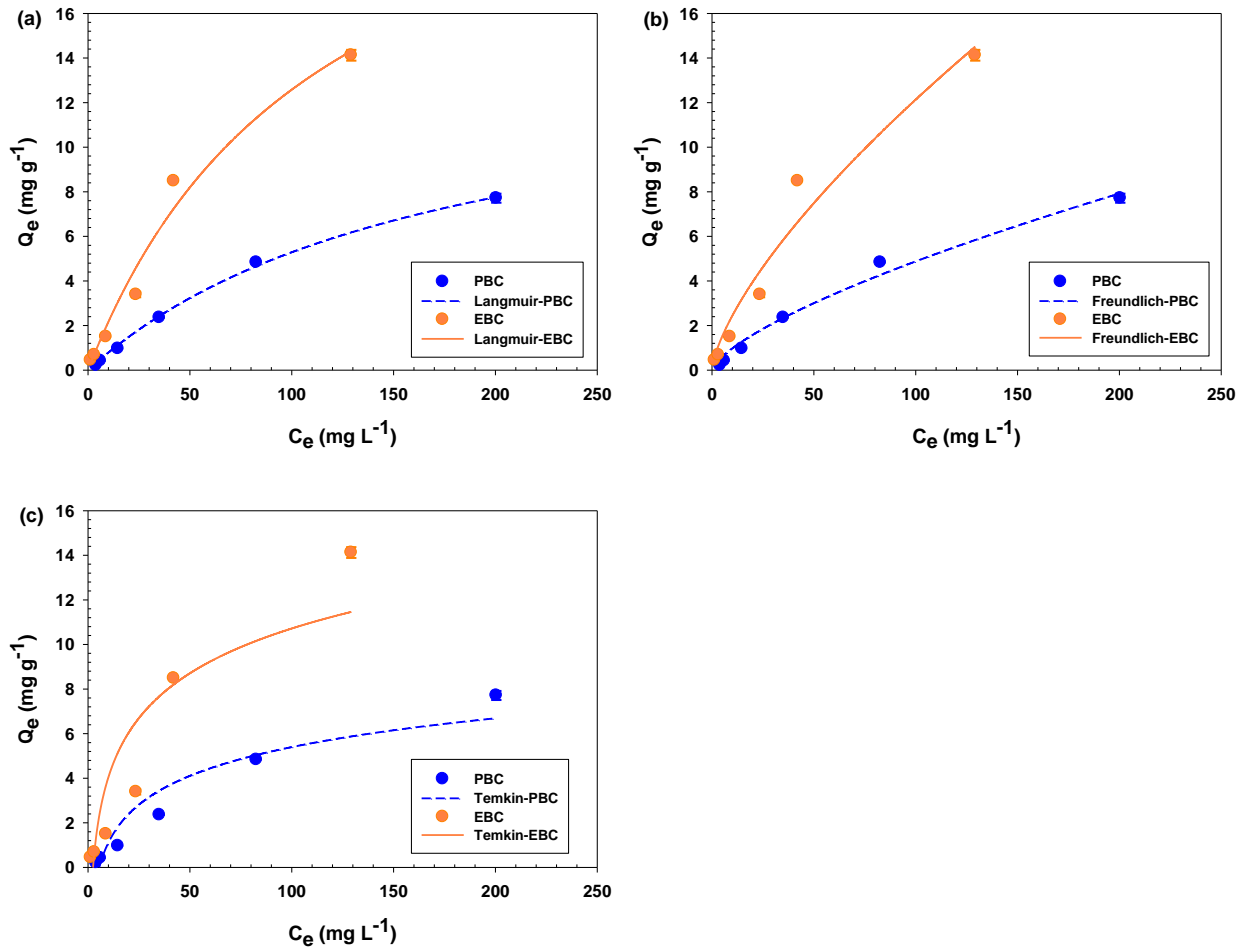
840



841

842 **Fig. 2:** The FTIR spectra of the pristine biochar (PBC) and the engineered biochar (EBC).

843

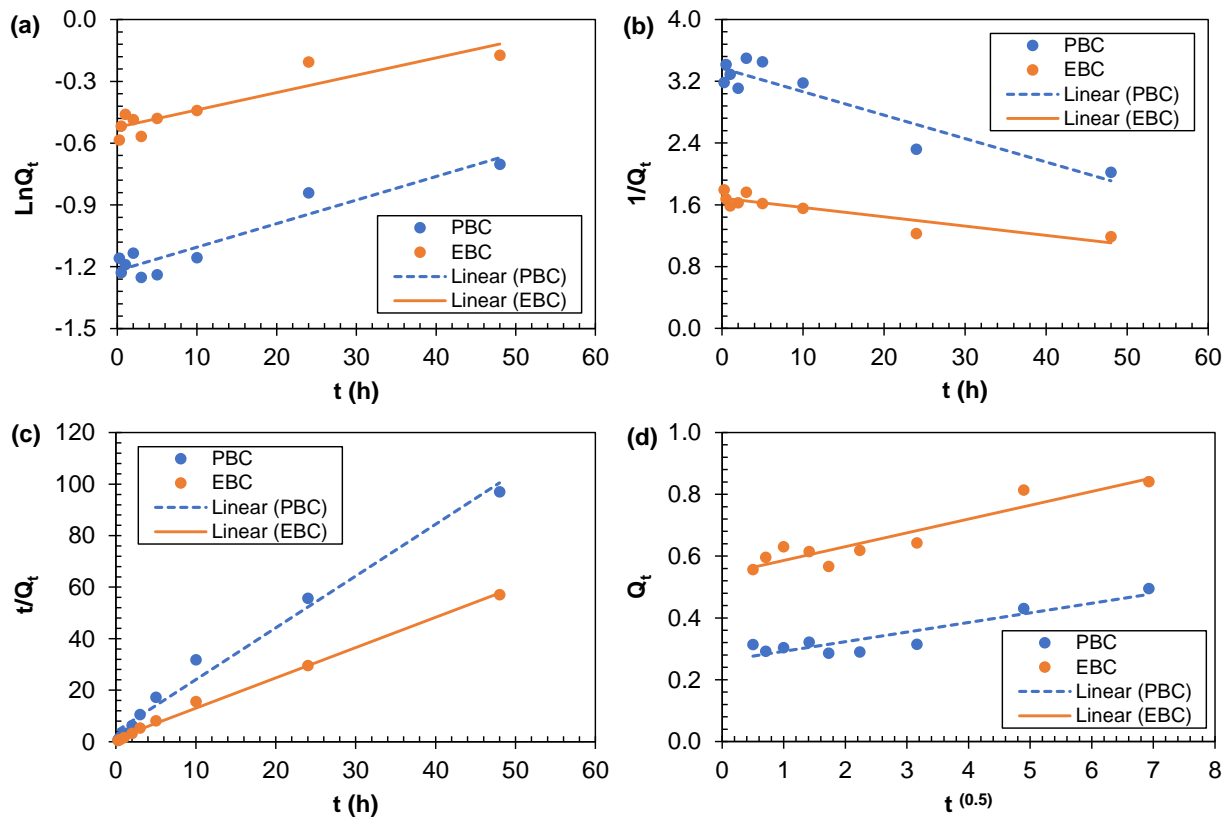


845

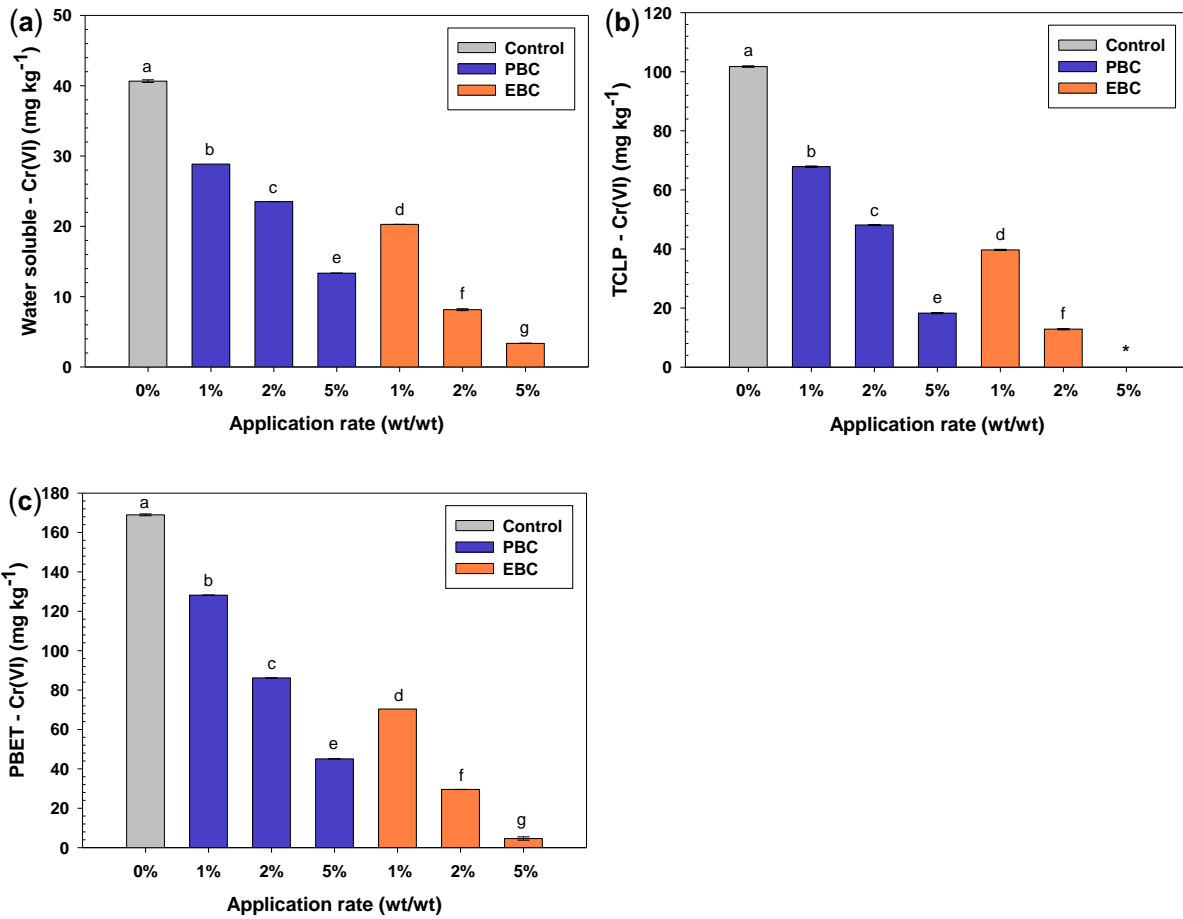
846 **Fig. 3:** Non-linear fittings of the (a) Langmuir, (b) Freundlich, and (c) Temkin isotherm models to the

847 experimental data of Cr(VI) adsorption onto the pristine biochar (PBC) and the engineered biochar (EBC).

848



849  
 850 **Fig. 4:** Linear fittings of the (a) first-order, (b) second-order, (c) pseudo-second order, and (d) intra-particle  
 851 diffusion kinetic models to the experimental data of Cr(VI) adsorption onto the pristine biochar (PBC) and  
 852 the engineered biochar (EBC).  
 853



854

855 **Fig. 5:** Effect of various application rates of the pristine biochar (PBC) and the engineered biochar (EBC)  
 856 on (a) water, (b) TCLP, and (c) PBET extracted Cr(VI) in contaminated soil. The similar letters on each bar  
 857 indicate non-significant differences between the different treatments at  $P < 0.05$  (\* = not detected).

858

859 **Supplementary material**

860 **A Remediation Approach to Chromium-Contaminated Water and Soil using Engineered**  
861 **Biochar Derived from Peanut Shell**

862

863 Hafiza Afia Murad<sup>a,1</sup>, Mahtab Ahmad<sup>a,1\*</sup>, Jochen Bundschuh<sup>b</sup>, Yohey Hashimoto<sup>c</sup>, Ming Zhang<sup>d</sup>, Binoy  
864 Sarkar<sup>e</sup>, Yong Sik Ok<sup>f,\*</sup>

865

866 <sup>a</sup> Department of Environmental Sciences, Faculty of Biological Sciences, Quaid-i-Azam University,  
867 Islamabad 45320, Pakistan

868 <sup>b</sup> UNESCO Chair on Groundwater Arsenic within the 2030 Agenda for Sustainable Development,  
869 University of Southern Queensland, West Street, Toowoomba, Queensland 4350, Australia

870 <sup>c</sup> Department of Bio-Applications and Systems Engineering, Tokyo University of Agriculture and  
871 Technology, 2-24-16 Koganei, Tokyo 184-8588, Japan

872 <sup>d</sup> Department of Environmental Engineering, China Jiliang University, No. 258 Xueyuan Street, Hangzhou,  
873 Zhejiang 310018, China

874 <sup>e</sup> Lancaster Environment Center, Lancaster University, Lancaster, LA1 4YQ, United Kingdom

875 <sup>f</sup> Korea Biochar Research Center, APRU Sustainable Waste Management Program & Division of  
876 Environmental Science and Ecological Engineering, Korea University, Seoul, Korea

877

878 <sup>1</sup> These authors share co-first authorship.

879

880 \* Corresponding authors

881 Email: [mahmad@qau.edu.pk](mailto:mahmad@qau.edu.pk) (Mahtab Ahmad); [yongsikok@korea.ac.kr](mailto:yongsikok@korea.ac.kr) (Yong Sik Ok)

882

883 **Analysis of column data**

884 The total adsorbed quantity of Cr(VI) ( $q_{\text{total}}$ ) was calculated from the following equation:

885 
$$q_{\text{total}} = \frac{QA}{1000} = \frac{Q}{1000} \int C_{\text{ad}} dt$$

886 where  $Q$  is the flow rate ( $\text{mL min}^{-1}$ ) of wastewater;  $A$  is the area under the curve, which was calculated  
887 through the integration of the plot of  $C_{\text{ad}}$  (adsorbed Cr(VI) concentration) versus  $t$  time (min). The total  
888 amount of Cr(VI) sent to column ( $M_{\text{total}}$ ) was calculated from the following equation:

889 
$$M_{\text{total}} = \frac{C_o Q t_{\text{total}}}{1000}$$

890 where  $C_o$  is the initial Cr(VI) concentration ( $\text{mg L}^{-1}$ ) fed to the column, and  $t_{\text{total}}$  is the total flow time (min).

891 The following equation was used to evaluate the column performance:

892 
$$\text{Removal (\%)} = \frac{q_{\text{total}}}{M_{\text{total}}} \times 1000$$

893 The column capacity or equilibrium Cr(VI) sorption ( $q_{\text{eq}}$ ) was calculated from the following equation:

894 
$$q_{\text{eq}} = \frac{q_{\text{total}}}{X}$$

895 where  $q_{\text{total}}$  is the total amount of Cr(VI) adsorbed in the column and  $X$  is the adsorbent amount (g) filled  
896 in the column.

897

898 **Table S1:** Selected properties of the experimental soil.

Parameter	Values
pH	5.00 ± 0.02
Electrical conductivity (dS m <sup>-1</sup> )	0.081 ± 0.00
Texture	Silt loam
Clay (%)	25.32 %
Silt (%)	53.98 %
Sand (%)	20.64 %
Organic matter (%)	0.93 ± 0.003
Water soluble phosphate (mg kg <sup>-1</sup> )	62.00 ± 0.71
Water soluble nitrates (mg kg <sup>-1</sup> )	26.33 ± 0.98
Total Cr (mg kg <sup>-1</sup> )	1992.23 ± 19.20
Cr(VI) (mg kg <sup>-1</sup> )	212.88 ± 15.06

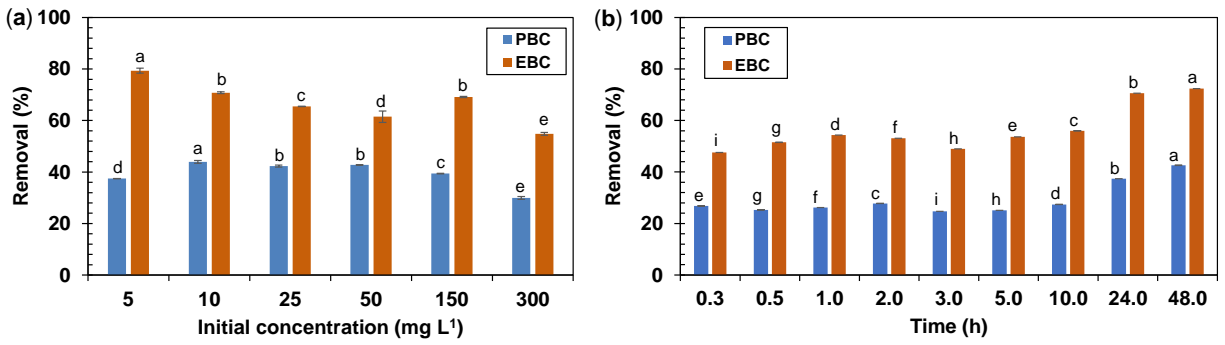
899

900

901 **Table S2:** Proximate analysis and physicochemical parameters of the pristine biochar (PBC) and the  
 902 engineered biochar (EBC).

Parameter	Values	
	PBC	EBC
Moisture (%)	3.34±0.19 <sup>a</sup>	2.49±2.44 <sup>b</sup>
Mobile matter (%)	24.11±0.56 <sup>a</sup>	20.15±0.35 <sup>b</sup>
Resident matter (%)	15.13±2.29 <sup>a</sup>	16.13±12.2 <sup>a</sup>
Ash (%)	57.42±1.93 <sup>a</sup>	59.63±4.31 <sup>a</sup>
pH	9.46±0.01 <sup>a</sup>	6.30±0.01 <sup>b</sup>
pH <sub>PZC</sub>	7.44±0.07 <sup>a</sup>	6.70±0.04 <sup>b</sup>
Electrical conductivity (dS m <sup>-1</sup> )	0.249±0.007 <sup>a</sup>	0.149±0.002 <sup>b</sup>
Organic matter (%)	1.66±0.33 <sup>a</sup>	1.15±0.34 <sup>b</sup>

903 The similar upper case letters on the values indicate non-significant differences at  $P < 0.05$  between the  
 904 two biochars.

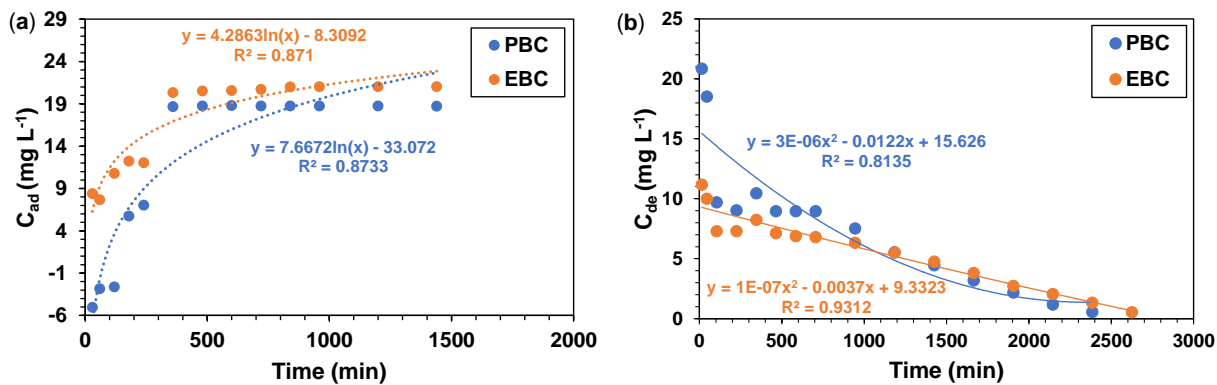


905

906 **Fig. S1:** Effect of (a) initial concentration and (b) contact time on percentage removal of Cr(VI) from water  
 907 by the pristine biochar (PBC) and the engineered biochar (EBC). The similar letters on the bars indicate  
 908 non-significant differences at  $P < 0.05$ .

909

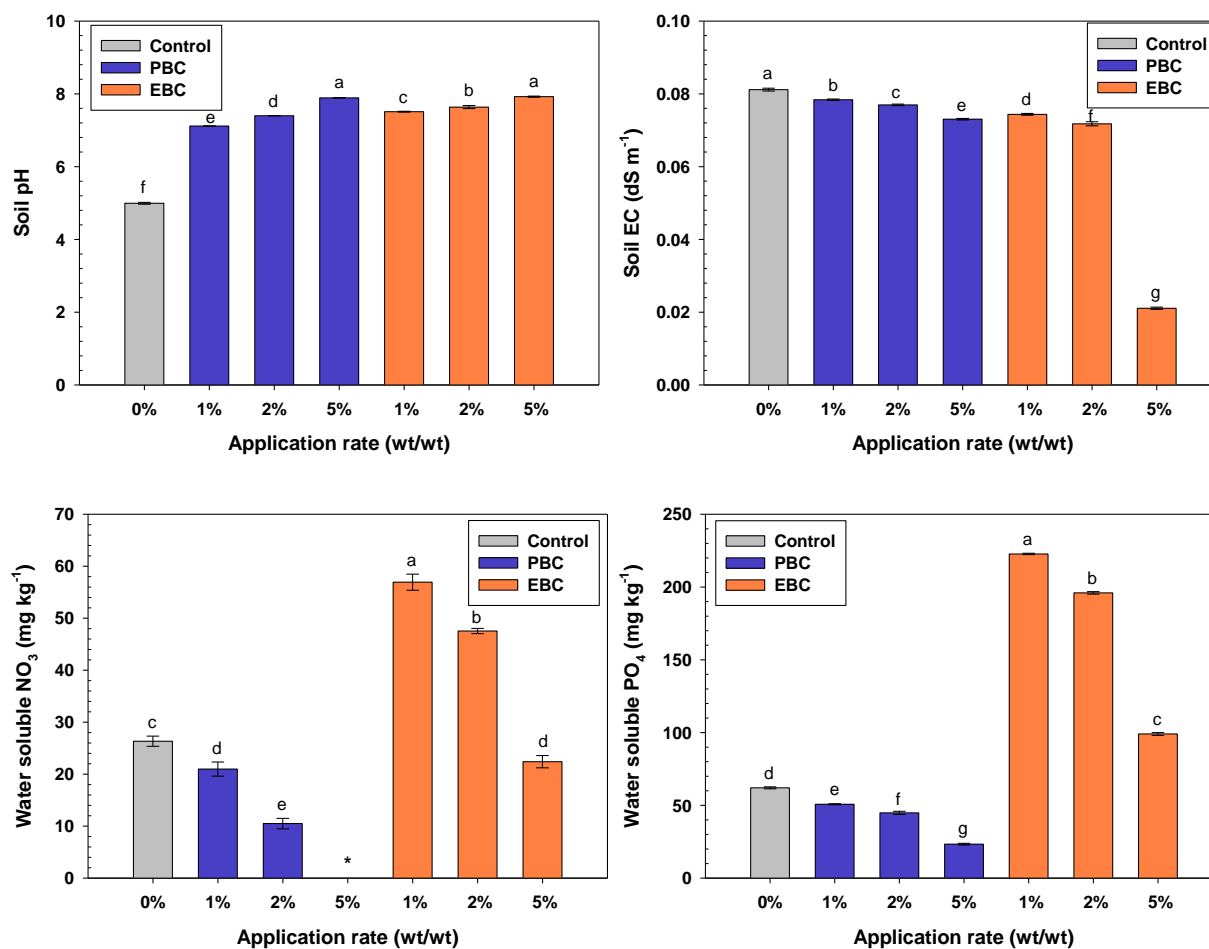
910



911

912 **Fig. S2:** (a) Adsorbed and (b) desorbed concentration of Cr(VI) as a function of time in a continuous fixed-  
913 bed column of the pristine biochar (PBC) and the engineered biochar (EBC).

914



915  
 916 **Fig. S3:** Effect of various application rates of the pristine biochar (PBC) and the engineered biochar (EBC)  
 917 on (a) soil pH, (b) soil EC, (c) water-soluble nitrates, and (d) water-soluble phosphates. The similar letters  
 918 on each bar indicate non-significant differences between the different treatments at  $P < 0.05$ .  
 919